Solving Sign Problems with Meron Cluster Algorithms: Simulating Field Theories at Non-Zero Chemical Potential

by

Benjamin S. Scarlet

A.B., Mathematics (1996)
Cornell University

Submitted to the Department of Physics
in partial fulfillment of the requirements for the degree of

Doctor of Philosophy

at the

MASSACHUSETTS INSTITUTE OF TECHNOLOGY

September 2000

Author .....
Department of Physics
August 24, 2000

Certified by .....
Uwe-Jens Wiese
Associate Professor of Physics
Thesis Supervisor

Accepted by .....
Thomas J. Greytak
Professor of Physics
Associate Department Head for Education

Solving Sign Problems with Meron Cluster Algorithms: Simulating Field Theories at Non-Zero Chemical Potential

by

Benjamin S. Scarlet

Submitted to the Department of Physics
on August 24, 2000, in partial fulfillment of the
requirements for the degree of
Doctor of Philosophy

Abstract

Numerical simulation of quantum systems develop sign problems upon the introduction of a chemical potential. The sign problem thus makes many interesting physical systems very difficult to study numerically. In this thesis, two related systems which develop sign problems in this way are considered: a D-Theory representation of a 1+1 dimensional O(3) quantum field theory with a chemical potential, and antiferromagnetic Heisenberg quantum spin ladders in a magnetic field. In both cases, meron cluster algorithms are used to completely solve the sign problem. Using these algorithms, numerical results were generated in the two models for, respectively, the particle number as a function of the chemical potential and magnetization as a function of the external field. These results are in agreement with corresponding analytic predictions.

Thesis Supervisor: Uwe-Jens Wiese
Title: Associate Professor of Physics

Acknowledgments

to my sister Leslie: for demonstrating perseverance in the face of true adversity;

to my parents Richard and Virginia: when I asked, "Why is the sky blue?" you answered, "Rayleigh scattering."

and to Meredith: for support, patience and proofreading.

Contents

List of Figures

List of Tables

Chapter 1

Introduction

1.1 Motivation from Strongly Coupled Systems

Many physical phenomena are described by strongly coupled systems. Nuclear and quark matter are described by strongly coupled quarks and gluons in quantum chromodynamics. High T_c superconductors are described by strongly coupled electrons. Magnets are described by strongly coupled spins. All these systems can be studied numerically, but current numerical techniques encounter serious inefficiencies for these models because of complex action problems.

1.1.1 Quantum Chromodynamics

Quantum chromodynamics (QCD) is the part of the Standard Model which describes the strong force. It describes hadrons and their interactions. It describes systems of hadrons such as nuclei. It describes more exotic systems which form when hadronic systems are subjected to extremes of temperature or density – such as the cores of neutron stars, the very early universe, and colliding heavy nuclei.

QCD is a theory of fermions called quarks interacting via the exchange of bosons called gluons which arise from an $SU(3)$ gauge symmetry called color. It is an asymptotically free theory – at sufficiently large energy scales it is weakly coupled, and so can be studied perturbatively. At smaller energies, however, the formerly weak inter-

actions become very strong, and the particles become bound up in intricate structures. The gluons are excluded from free space – like a magnetic field from a superconductor – and so they form flux tubes connecting the color-charged quarks. The quarks, now bound together by a force which does not decrease with their separation, form tightly bound collectives with no net color charge: hadrons.

This rudimentary description suffices to motivate the theory, but it is incomplete and oversimplified. The range of theorized phenomena which may occur in quark and gluon physics is both broadly varied and deeply complex. It includes not only the qualitative picture of confinement described above, but also more exotic phenomena. A color-superconducting phase is theorized to exist at extreme densities, perhaps in neutron stars [3, 44]. A quark-gluon plasma is theorized to exist at high temperature and high density; such a plasma may be created in heavy ion collisions at RHIC, for example [43]. In order to study the strongly coupled regime in sufficient detail to understand these phenomena it is necessary to use quantitative, non-perturbative techniques.

The most prominent such method is Monte Carlo lattice simulation. This technique is effective for studying QCD at finite temperatures but zero chemical potential, and so exploring its phase transitions and attempting better to understand the phenomenon of confinement. For finite density, however, when a chemical potential is necessary, current Monte Carlo techniques are not effective. The introduction of chemical potential causes Monte Carlo simulation to become very inefficient because complex action problems develop. Thus the realm of the phase diagram away from zero chemical potential is currently inaccessible to numerical study. At extremely large chemical potential, the typical energy scale (determined by the Fermi energy) becomes large enough that the coupling descends into the perturbative regime. Unfortunately, the density range which can be treated this way is impractically dense – far denser than nuclear matter.

1.1.2 High T_c Superconductors

Some layered cuprates, such as La_2CuO_4, exhibit high T_c superconductivity when appropriately doped with barium. These materials can be modeled as two dimensional lattices of strongly coupled electrons because the coupling between layers is relatively weak. Before doping, these materials exhibit the symmetry breaking pattern of the Heisenberg antiferromagnet: $SO(3) \to SO(2)$ producing two Goldstone modes: magnons. After doping, when superconductivity appears, they instead exhibit a different pattern: the $U(1)$ gauge group of electromagnetism breaking completely. The mechanism by which superconductivity develops in these materials is not at present understood; phonon exchange is not the phenomenon responsible for the formation of Cooper pairs.

When undoped, these strongly coupled systems can be modeled effectively and efficiently as a Heisenberg antiferromagnet [5], yet the qualitative changes induced by doping the system necessitate the use of a different model. The Hubbard model is a candidate to fill this role, but in order to represent the doped materials it is necessary to introduce a chemical potential. For the Hubbard model as with QCD, the zero chemical potential case can be effectively simulated, but when a chemical potential is introduced a sign problem develops.

1.1.3 Antiferromagnets

A much simpler and better understood system, the quantum Heisenberg antiferromagnet, is also a strongly coupled system which can be studied numerically. It is a lattice of quantum spins with a global $O(3)$ symmetry interacting through an antiferromagnetic nearest-neighbor coupling. In this case an external magnetic field, with which the spins tend to align, plays the role of a chemical potential. As in the other systems, when the field is switched on traditional Monte Carlo methods become inefficient.

Interestingly, in this case it is not immediately apparent that a sign problem is involved in the inefficiency which develops in simulation. With the simplest choice of

quantization axis – along the magnetic field – the inefficiency appears in a different form. Only when one makes a counterintuitive choice for the quantization axis – transverse to the field – is the inefficiency forced to manifest itself as a sign problem. This choice at first appears ill made precisely because it leads to a sign problem (a known source of difficulty), and so it seems a poor way to simulate the magnet. However, for the purpose of exploring the sign problem this choice is very favorable. By subsequently solving the sign problem, one can circumvent the original inefficiency and so the model can be effectively simulated.

1.2 D-Theory

Models for systems such as these are usually formulated in terms of path integrals. A Boltzmann weight is formed from a classical Euclidean action in the case of Euclidean field theory, or from a classical or quantum Hamiltonian in the case of statistical mechanics. This Boltzmann weight is in turn integrated over all physical configurations to yield a partition function. The partition function generates all observables. *D-Theory* is a new modified formulation of quantum field theory in which the usual continuous fields arise from discrete variables that undergo dimensional reduction.

1.2.1 An Extra Quantization

The formal similarity between a classical Hamilton function and a classical Euclidean action is commonly exploited to draw an analogy between classical statistical mechanics and quantum field theory. By further exploiting that analogy, one can construct a second possibility for quantum field theories: using a "quantum" Euclidean action. Just as a quantum Hamiltonian can be formed from a classical one by promoting variables to operators, so can a quantum Euclidean action be formed from a classical one. These operators act in a new Hilbert space.

- Just as a traditionally formulated field theory uses a classical action analogous to a classical Hamiltonian in classical statistical mechanics; so this new formulation

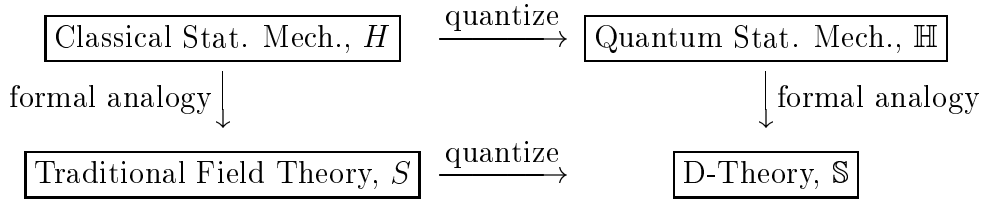

Figure 1-1: *The relationship of the D-Theory formulation to traditional field theory and statistical mechanics.*

of field theory uses an action which is an operator analogous to a quantum Hamiltonian operator in quantum statistical mechanics.

- Just as a system in quantum statistical mechanics can have a classical limit reproducing the corresponding system in classical statistical mechanics; so can this new system with an action operator have a limit which reproduces the original quantum field theory with the classical action.

The analogy between D-Theory and quantum statistical mechanics is useful, but it is not perfect. In quantum statistical mechanics, one usually has the luxury of being interested, finally, in the quantum system. In D-Theory, one is interested not in the newly quantized system but in the original quantum field theory with a classical action. Thus one must somehow recover some classical limit of the new system. Moreover, just as the action of a quantum Hamiltonian may be interpreted as generating translations through time, so may the action of this new D-Theory quantum action be interpreted as generating translations through a new dimension. In order to recover the original system, one must somehow dispose of this new dimension.

1.2.2 Dimensional Reduction

The original system can be recovered by exploiting the phenomenon of *dimensional reduction*. When a $D+1$ dimensional system is formulated at finite temperature, and the correlation length can be made significantly larger than the extent of the last dimension, then the system can be caused to behave effectively like a system of one less dimension but of the same symmetry class. Under these circumstances,

the thickness of the system in the $(D+1)$st direction is reduced to be very small in the physical units determined by the correlation length. Presuming the limit may be taken in such a way that the other dimensions do not also disappear, the system becomes effectively D dimensional and so is said to be dimensionally reduced.

The process of dimensional reduction does not affect the symmetry properties of the system, and so the low energy effective theory which describes the system after dimensional reduction will have the same symmetries as the quantized Euclidean action. The quantized action, by construction, has the same symmetries as the original classical action. Thus the effective theory after dimensional reduction should be in the same universality class as the original action, and so to this extent the original system can be recovered.

It may seem strange that one would decide to add an extra dimension to a system to be simulated, as the computing time necessary is heavily dependent on the volume of the system simulated. The benefits which can be derived from the use of the discrete variables in a quantized system, however, are very significant.

1.2.3 A Useful Example: (1+1+1)D $O(3)$

Consider the aforementioned Heisenberg quantum antiferromagnet, in the case of 2+1 dimensions. At low temperature the system develops long range order, and the global $O(3)$ symmetry breaks down to $O(2)$. The dynamics of the system with broken symmetry are described by two Goldstone modes – perturbations around the broken ground state in the coset space $O(3)/O(2) = S^2$. In fact, the correlation length is exponentially dependent on the extent of the third dimension. For an appropriate temperature, the extent of the third dimension will become negligible and the resulting system may then be interpreted as a (Euclidean) 1+1 dimensional system. Thus the system reduces to a 1+1 dimensional quantum field theory of a unit vector field – i.e. (1+1)D $O(3)$. This is a well understood system, and has some properties which make it a good toy model for QCD: it is asymptotically free and it has a mass gap.

1.2.4 Application to QCD

D-Theory formulations also exist for gauge theories. It is necessary that one find operators with suitable commutation relations to serve as promotions of the classical variables, and it is necessary that the correlation in the resulting system may be made significantly larger than the extent of the extra dimensional. Through the use of quantum link models, systems satisfying these constraints have been found for $U(1)$, $SU(2)$ gauge theories, and for QCD, including quarks [13, 19].

1.3 The Sign Problem

Traditionally formulated numerical lattice studies [25] generally encounter significant technical problems when a chemical potential is introduced. These methods are statistical, using Monte Carlo integration: they estimate physical quantities by averaging contributions randomly selected from a vast space of possibilities. Once a chemical potential is introduced, the individual contributions fluctuate much more dramatically, varying not only in magnitude but in phase or sign: the method develops a sign problem. These additional fluctuations introduce so much noise to the averages that in order to produce meaningful answers it would be necessary to generate samples of a size exponential in the volume of the system. Samples of such a large size are prohibitively expensive to generate, and so these traditional methods are not practical.

Because of the sign problem, the useful tool of lattice study is unavailable for systems with a chemical potential. As demonstrated above, the list of such systems includes several which are of significant interest. A method to circumvent the sign problem could allow lattice studies of all these systems, and so provide answers to many questions about them.

A different, more intricate formulation for Monte Carlo integration, *cluster algorithms*, may provide such a method. Cluster algorithms make greater use of the structure of the model to which they are applied than traditional methods, and as such they are more difficult to devise for any particular system. Once constructed,

they provide a rich environment for further work because the algorithm is closely tied to the physics of the system being simulated. Recently, cluster algorithms have been used to solve sign problems in some fermion models [20, 17]. In these cases, the sign problems arise not because a chemical potential is introduced, but because of the anticommuting nature of the fermions. It shall be shown below that cluster algorithm framework can be used also to solve the sign problems which arise due to the introduction of a chemical potential.

Cluster algorithms are much easier to construct for systems whose local degrees of freedom are discrete. In fact, there are extremely few known cases of any cluster algorithm for which the local degrees of freedom are continuous. With this in mind, one can see the advantage of the D-Theory representation. It may be possible to implement cluster algorithms for a broader range of symmetry classes by formulating them with D-Theory in terms of discrete local degrees of freedom. Unfortunately, no effective cluster algorithm is yet known for gauge theories formulated in terms of D-Theory. The lack of efficient cluster algorithms for gauge theories is a significant hurdle remaining between the techniques presented here and their application to QCD.

Chapter 2

Background

2.1 Algorithms

In numerical simulations of field theories, the field theory is regularized on a space-time lattice. Crystal structures like the magnet exist on a lattice a priori. In either case, the core computational task in such a simulation is to evaluate integrals generated by the partition function over the enormous space of all field configurations on the lattice.

2.1.1 Constructing the Path Integral

Time Slices

Given a Hamiltonian operator $\mathbb{H}$, either from quantum statistical mechanics or from an analogous D-Theory quantized action $\mathbb{S}$, the partition function Z is given by $Z = \mathrm{Tr}\left(e^{-\beta\mathbb{H}}\right)$. In order to express the action of $\mathbb{H}$ over the extent β in a manageable form, it is split into N slices of thickness ϵ. Between each pair of slices an explicit state of the system is inserted. Now

$$Z = \mathrm{Tr}\left(e^{-\beta\mathbb{H}}\right) = \mathrm{Tr}\left(e^{-\epsilon\mathbb{H}}\right)^N = \int [D\psi] \prod_{t=1}^{N} \langle\psi_{t+1}|e^{-\epsilon\mathbb{H}}|\psi_t\rangle, \tag{2.1}$$

where the integral is over all values of each ψ_t.

Trotterization

The action of the Hamiltonian, even in one slice, remains difficult to analyze because everything across the whole system happens at once. Thus one introduces a *Trotter decomposition*, taking advantage of the locality of the Hamiltonian. In terms of the lattice, locality implies that sites interact only with nearby sites. For the purposes of this thesis, it will be sufficient to consider only square lattices with nearest-neighbor couplings. The ideas presented here are readily generalizable to more complex scenarios. The Hamiltonian can now be written as $\mathbb{H} = \sum_{x,\mu} \mathbb{H}_{x,\mu}$, where μ runs over all directions – unit vectors aligned with the lattice – $(+\hat{x}_0, +\hat{x}_1, \ldots, -\hat{x}_0, -\hat{x}_1, \ldots)$, and x correspondingly runs for each μ over half the sites on the lattice, so that the pairs of sites $(x, x+\mu)$ cover the whole lattice. Note that $\mathbb{H}_{x,\mu}$ and $\mathbb{H}_{y,\nu}$ will not commute when the pairs of sites acted upon by each share a site, but $\mathbb{H}_{x,\mu}$ and $\mathbb{H}_{y,\mu}$ must commute. Now the locality of the Hamiltonian can be exploited by expanding the exponential:

$$e^{-\epsilon \mathbb{H}} = e^{-\epsilon \sum_{x,\mu} \mathbb{H}_{x,\mu}} \approx \prod_{\mu} e^{-\epsilon \sum_{x} \mathbb{H}_{x,\mu}} = \prod_{\mu} \left(\prod_{x} e^{-\epsilon \mathbb{H}_{x,\mu}} \right) \tag{2.2}$$

The Trotterization step does introduce errors at order ϵ^2, but for sufficiently small ϵ the approximation can be made acceptable.

In principle, it is not necessary to use the Trotter decomposition or even to discretize the time direction at all. For some cluster algorithms, it is possible to work directly in continuous Euclidean time [8]. Such algorithms are significantly more difficult to implement, and the improvement they offer is chiefly in speed rather than insight. Since the latter was the purpose of this thesis, the Trotter scheme was chosen.

An Easily Representable Lattice

With the action of the Hamiltonian thus broken down, the partition function can now be written as

$$Z = \int [D\psi] \prod_{t=1}^{N} \langle \psi_{t+1} | \left(\prod_{\mu} \prod_{x} e^{-\epsilon \mathbb{H}_{x,\mu}} \right) |\psi_t\rangle \tag{2.3}$$

$$= \int [D\psi] \prod_{t,\mu,x} \langle \psi_{t',\mu',x} | \langle \psi_{t',\mu',x+\mu} | e^{-\epsilon \mathbb{H}_{x,\mu}} |\psi_{t,\mu,x}\rangle |\psi_{t,\mu,x+\mu}\rangle. \tag{2.4}$$

Given t and μ, t' and μ' specify the next slice. Except when μ is the last direction, $t' = t$ and μ' is the direction after μ. When there is no next μ, μ' reverts to the first direction and $t' = t + 1$. The operator

$$\mathbb{T}_{t,\mu,x} = e^{-\epsilon \mathbb{H}_{x,\mu}} \tag{2.5}$$

is called the *transfer matrix*. The corresponding element of this matrix in a particular configuration ψ is written

$$T_{t,\mu,x} \equiv \langle \psi_{t',\mu',x} | \langle \psi_{t',\mu',x+\mu} | \mathbb{T}_{t,\mu,x} |\psi_{t,\mu,x}\rangle |\psi_{t,\mu,x+\mu}\rangle. \tag{2.6}$$

$\mathbb{T}$ is a local quantity of manageable size, and so the partition can finally be written as

$$Z = \int [D\psi] \prod_{t,\mu,x} T_{t,\mu,x} \tag{2.7}$$

where the integral runs simply over all states of each site in the Trotterized lattice.

The Structure of the Transfer Matrix

The transfer matrix $\mathbb{T}$ on any given plaquette is a actually a four index tensor $\mathbb{T}_{i,j;k,l}$. There are two ways in which two objects like the transfer matrix can me multiplied, corresponding to the two directions defining its plaquette. Given another such

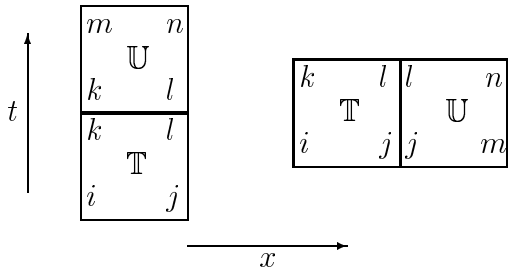

Figure 2-1: *The two multiplications for transfer matrices. The time-like and space-like multiplications correspond to time-like and space-like concatenation of plaquettes.*

object $\mathbb{U}$, the two may be multiplied in time-like order, as

$$(\mathbb{U}\mathbb{T})_{m,n;i,j} = \mathbb{U}_{m,n;k,l}\mathbb{T}_{k,l;i,j} \tag{2.8}$$

or in space-like order, as

$$(\mathbb{U} \star \mathbb{T})_{k,n;i,m} = U_{l,n;j,m}T_{k,l;i,j}. \tag{2.9}$$

If a transfer matrix is written out as a matrix – so that its indices are paired up to produce a two index object – there are two valid pairings, one for each multiplication. Usually, but not always, the pairing for time-like multiplication shall be used.

Making Measurements

The partition function is a generating function for physical observables. Generally, one extracts actual physical quantities from the partition function by differentiating $\ln Z$ and hence bringing some quantity of interest down into the integral out of the Hamiltonian. In the end, one is interested in calculating

$$\langle \mathcal{O} \rangle = \frac{1}{Z} \int [D\psi]\, \mathcal{O}[\psi] \prod_{t,\mu,x} T_{t,\mu,x} \tag{2.10}$$

for some observable $\mathcal{O}$. Both the integral for these measurements and Z itself are thus all of the form

$$\int [D\psi]\, \mathcal{O}[\psi] \prod_{t,\mu,x} T_{t,\mu,x} \tag{2.11}$$

with $\mathcal{O} \equiv 1$ for Z.

2.1.2 Importance Sampling

Because the domain of these integrals is huge, it is impractical to use most simple numerical integration techniques. Instead, one takes advantage of the sharply peaked nature of the integrand arising from its exponential form. This property renders the integral susceptible to approximation by importance sampling techniques: one generates an ensemble of representative configurations from the integration domain, chosen to be distributed according to their significance in contributing to the integral. Because of the relation between the distribution of configurations and their relative significance, a sample of a reasonable size from the ensemble is sufficient to make a decent approximation of the integral even though such a sample covers only a miniscule fraction of the whole integration domain.

Once a distribution is determined, it is necessary to generate from it some finite ensemble. The usual method for generating the ensemble is to use a Markov process. The distribution assigns a Boltzmann weight to every configuration. One takes a random walk through the configuration space, choosing each step according to the weights. As a particle walking randomly in a potential spends most time at the bottom, so such a walk spends most of its time in configurations with the greatest Boltzmann weight. When taken as an orderless collection, the set of states visited is the ensemble.

To use a Markov process, it is necessary only to find some method of taking steps which satisfies both ergodicity and detailed balance. These two requirements guarantee first that a walk may in principle reach any configuration, and second that a step between any two states respects the relative weights of two. Taken together, the two

requirements guarantee that a walk will eventually generate the desired distribution.

2.1.3 Metropolis

The most common method for taking Markov steps is a local Metropolis algorithm. The local Metropolis algorithm has the advantages both of being relatively simple and of being widely applicable. It has the disadvantage of long autocorrelation time – it makes only small changes to the lattice in each step, and it may make no change at all. Because the steps taken through a very large configuration space are very small, the Metropolis algorithm necessarily takes many steps to walk between any two given configurations.

Given a starting configuration for a step, one picks a point on the lattice, generates a random new state for that point, and proposes the new configuration as the next step. By comparing the new and old Boltzmann weights, one determines a probability with which the new configuration should be accepted. One then chooses according to that probability either to accept or to reject the proposal. If the proposal is accepted, the configuration added to the walk is the one with the changed state. If the proposal is rejected, the configuration added is the same as the previous one.

2.1.4 Clusters

In contrast, a more advanced method of taking Markov steps is to use a cluster algorithm. Cluster algorithms have the advantage of having short autocorrelation times. Because each step makes broad changes affecting large regions of the lattice these algorithms can move between any two states in configuration space in relatively few steps. Cluster algorithms have the disadvantages of being complicated and, more importantly, of being difficult to devise. Constructing a cluster algorithm for a given physical system remains something of a black art.

Given a starting configuration, one breaks up the volume into regions called *clusters* according to *cluster rules* which bond together sites on the lattice. Then one performs some *cluster flip* on each cluster. A cluster flip is some change of each state

in the cluster, coordinated across the entire cluster. In a two state model it might be flipping every spin in a cluster or it might be doing nothing; in a classical spin model with continuous spins it might be reflecting all spins in a cluster across a given plane. The cluster rules determine which elements of the lattice may be bound together into the same cluster. Moreover, it is required of the rules that, once the clusters are chosen, a randomly chosen flip will necessarily be acceptable.

For a partition function of the general form $Z = \int [D\psi] W[\psi]$, the integral of interest for an observable $\mathcal{O}$ is

$$\int [D\psi] \mathcal{O}[\psi] W[\psi]. \tag{2.12}$$

A cluster algorithm can be viewed as an expansion of the configuration space of a system. To the physical degrees of freedom, new local variables are added called *breakups* which describe the cluster connections. Breakups exist on the same elements of the lattice as the transfer matrix – in the cases here, on plaquettes. They can be envisioned as patterns of bonds between sites in a plaquette – choices of how to connect nearby lattice elements and so to break up the lattice into clusters. Cluster algorithms thus *differentiate in*[1] new breakup degrees of freedom b on each plaquette, so that

$$\int [D\psi]\, [Db]\, \mathcal{O}[\psi] W[\psi, b]. \tag{2.13}$$

$W[\psi, b]$ is restricted to take the form

$$W[\psi, b] = \delta[\psi, b] W[b] \tag{2.14}$$

where $\delta[\psi, b] \in \{0, 1\}$, which implies that

$$\int [Db] W[\psi, b] = W[\psi]. \tag{2.15}$$

[1] the opposite of integrating out

The remaining details of the breakups are left to be determined by the physics of the system: precisely what constraint between sites a bond implies, what patterns of bonds are allowed, and with what frequency each pattern appears. The clusters are the percolated sets of bonds and sites into which the bonds break up the lattice.

The details of δ encode a sense of satisfiability – a given physical configuration either does or does not satisfy a given cluster configuration. δ can be further broken down, as it may enforce constraints only upon sites which are bonded together. Thus when a given configuration of breakups b results in a set of N_b clusters $C_b = c_1, c_2, \ldots, c_{N_b}$, δ can be written

$$\delta[\psi, b] = \prod_{n=1}^{N_b} \delta_{c_n} \tag{2.16}$$

where $\delta_{c_n} = 1$ if all the bonds in cluster c_n are satisfied, and $\delta_{c_n} = 0$ otherwise. Of course, any term in the path integral for which any δ_{c_n} is zero will drop out, and the terms which remain can be described by independently varying each cluster over a set of states for its sites which satisfy its bonds.

The integral can be reinterpreted in this light, putting the cluster structure foremost:

$$\int [Db]\, W[b] \int [D\psi]\, \delta[\psi, b] \mathcal{O}[\psi] \tag{2.17}$$

$$= \int [Db]\, W[b] \int [D\psi] \prod_{n=1}^{N_b} \delta_{c_n} \mathcal{O}[\psi] \tag{2.18}$$

$$= \int [Db]\, W[b] \int \left(\prod_{n=1}^{N_b} d\psi_{c_n} \right) \mathcal{O}[\psi]. \tag{2.19}$$

Here ψ_{c_n} represents the state of the cluster c_n. Finally, the original integral over all states of the lattice has been rewritten as an integral over all clusters on the lattice and all states of those clusters.

2.2 The Sign Problem Revisited

Metropolis algorithms for numerical study of lattice theories encounter significant problems when a chemical potential is introduced. In particular, the introduction of the chemical potential generally causes a *complex action problem* or *sign problem*. Despite differences between the details in the formulations of different theories, a general pattern still exists: while the chemical potential is zero, the phase of the integrand in the partition function is constant over the integration domain; once the chemical potential introduces a non-zero charge, the phase is no longer constant. The details of the mechanism by which the varying phase is introduced can differ greatly between models, but the result is the same: if the importance sampling technique is used unmodified, the varying phase of the integrand leads to a very serious signal-to-noise problem.

2.2.1 What Goes Wrong

When the chemical potential is zero, the Euclidean action of a field theory is real. The integrand in eq. (2.7) is correspondingly both real and positive, and so, for a well behaved observable, the phase of the integrand in eq. (2.10) can be factored out of the integration. The remaining integration is then one of positive real quantities, and it can proceed with no cancellations.

When the chemical potential introduces a non-zero charge, however, the action of a field theory will, in general, become complex. Correspondingly, after the construction of the path integral and Trotterization, the elements of the transfer matrix will pick up signs or phases. The phase of the integrand – now changing from configuration to configuration within the integration domain – must be included in the observable to be averaged over the integration domain. Of course, a less well behaved observable which is not always real and positive could also introduce a sign problem.

In order to continue to make use of importance sampling in the presence of these varying phases, the integrals can be rewritten in terms of a strictly positive real

weight:

$$\int [D\psi]\, \mathcal{O}[\psi] \prod_{t,\mu,x} T_{t,\mu,x} \equiv \int [D\psi]\, \mathcal{O}[\psi] \mathrm{sign}[\psi] W[\psi] \tag{2.20}$$

where

$$W[\psi] \equiv \left| \prod_{t,\mu,x} T_{t,\mu,x} \right| \qquad \text{and} \qquad \mathrm{sign}[\psi] \equiv \left(\prod_{t,\mu,x} T_{t,\mu,x} \right) W^{-1}[\psi]. \tag{2.21}$$

This new Boltzmann weight W can be thought of as arising from the action of a modified system in which the transfer matrix elements are forced to be real and positive. Denoting by $\langle \mathcal{O} \rangle_m$ the expectation value of an observable in this modified ensemble, an expectation value in the original ensemble can now be calculated as

$$\langle \mathcal{O} \rangle = \frac{1}{Z} \int [D\psi]\, \mathcal{O}[\psi] \prod_{t,\mu,x} T_{t,\mu,x} \tag{2.22}$$

$$= \frac{\int [D\psi]\, \mathcal{O}[\psi] \mathrm{sign}[\psi] W[\psi]}{\int [D\psi]\, \mathrm{sign}[\psi] W[\psi]} \tag{2.23}$$

$$= \frac{\langle \mathcal{O}[\psi] \mathrm{sign}[\psi] \rangle_m}{\langle \mathrm{sign}[\psi] \rangle_m}. \tag{2.24}$$

The average of the sign in the modified ensemble is a ratio of the two partition functions:

$$\langle \mathrm{sign}[\psi] \rangle_m = \frac{1}{Z_m} \int [D\psi]\, \mathrm{sign}[\psi] W[\psi] = \frac{Z}{Z_m} = e^{-\beta V \Delta f}. \tag{2.25}$$

Thus, since $Z_m \geq Z$, $\langle \mathrm{sign}[\psi] \rangle_m$ is exponentially small in both β and V. The individual contributions from single configurations, however, do not diminish so dramatically with the volume. The small magnitude of the average is a result of the averaging process itself – the result is small because of cancellations between terms which are not so small.

If Monte Carlo methods are applied directly to calculate the integrals in eq. (2.23), simply using W to determine an importance sampling ensemble, then these cancellations lead to unacceptable errors. Since individual contributions to the integral

are chosen probabilistically according to their magnitude without consideration of the cancellation process, particular cancellations do not necessarily occur. A term may be present in the estimating sum while a canceling partner to that term is not present. Because individual terms are dramatically larger than the final average, the error contributed to the estimate by a single uncancelled term overwhelms any meaningful result from a simulation. The relative error in $\langle \text{sign} \rangle_m$ is

$$\frac{\Delta \text{sign}}{\langle \text{sign} \rangle_m} = \frac{\sqrt{\langle \text{sign}^2 \rangle_m - \langle \text{sign} \rangle_m^2}}{\sqrt{N} \langle \text{sign} \rangle_m} \approx \frac{e^{\beta V \Delta f}}{\sqrt{N}}. \tag{2.26}$$

Thus $\langle \mathcal{O} \rangle$, while itself of order 1, has wound up being calculated as a ratio of two quantities which are exponentially small relative to their respective errors. While extremely large statistical samples (exponentially large as a function of the volume) could in principle overcome this signal-to-noise problem, such exponentially large samples are prohibitively expensive and so not practical.

2.2.2 A Scheme to Build a Solution

Fortunately, the signal-to-noise problems which occur in this simplest application of Monte Carlo methods are not endemic to the physics or even to the importance sampling technique – other formulations may succeed where the simplest has failed. The method presented in this thesis uses such a new formulation. It uses cluster techniques and the notion of improved estimators to generate a more intelligently chosen ensemble, in which the cancellation problems do not occur.

The direct method fails because the importance sampling ensemble has become corrupted. Configurations which generate contributions of large magnitude to the integrand are all considered important, yet in most cases their contribution eventually will be canceled out.

If some greater organization can be imposed upon the domain of integration, classifying configurations into small groups most of which will cancel out internally, then a more useful ensemble may be generated. Given such a classification scheme,

the importance of configurations which will cancel out in the end can be understood to be much less than their absolute magnitude would imply. By suppressing the occurrence of such configurations in the distribution which determines the estimating ensemble, one can drastically reduce the variance of the estimate of the integral.

Once one has a classification scheme, one can construct an *improved estimator*. An improved estimator for an observable averaged over an ensemble is a different observable with the same ideal average but which varies less widely between individual elements of the ensemble. In the idealized limit of a very large ensemble, an improved estimator will, by definition, average out to the same result as would the original observable; in a more realistic representative but finite ensemble, averaging the improved estimator will yield a better estimate of the ideal average – one with a lesser variance.

Given an appropriate classification scheme, an improved estimator can be constructed using a simple procedure. The domain of the average is broken down into many small subdomains by the classification scheme. Over each such subdomain, one must be able to calculate the average explicitly. The value of the improved estimator for any state shall be the average over the sub-domain in which the state sits. If the scheme is constructed as described above – so that usually the phases within a group cancel – then the value of the improved estimator will be zero on most of the configuration space. That these zeroes can be uncovered is a reflection of the nature of the sign problem – what was previously a jumble of large contributions canceling out to a small result is now a set of pre-averaged pieces, most of which contribute nothing. Once the improved estimator has uncovered the cancellation, the importance sampling distribution can be modified to reflect the true significance of each configuration.

In order to apply this method, one must find an appropriate classification of the configuration space into subdomains over which one can perform the average explicitly. This thesis shall demonstrate that the use of cluster techniques can provide a framework in which the physical symmetries of the system can be exploited to find a natural and effective choice of subdomains.

2.2.3 Improved Estimators from Cluster Algorithms

Cluster algorithms provide an excellent foundation upon which to construct improved estimators as described above. Once the configuration space has been expanded to include not only the physical degrees of freedom but also the breakups, a classification scheme for constructing improved estimators is readily apparent: All joint configurations with the same cluster configuration shall be grouped together into a subdomain. Improved estimators can then be constructed as the average over all cluster orientations for a given cluster configuration.

Eq. (2.19) has the form necessary for an improved estimator for the integral in eq. (2.12). If the inner integral – the integral over the states of each cluster in a given cluster configuration – can be performed explicitly, then an improved estimator will be available. Given a cluster configuration b, it is necessary that it be possible to calculate

$$\mathcal{O}[b] \equiv \int \left(\prod_{n=1}^{N_b} d\psi_{c_n} \right) \mathcal{O}[\psi]. \tag{2.27}$$

If the number of clusters in any given configuration becomes large, integrals such as this one will not necessarily be easy – there will still be too many variables to integrate at once. However, if the observable $\mathcal{O}$ can be factored so that

$$\mathcal{O}[\psi] = \prod_{n=1}^{N_b} \mathcal{O}_{c_n}(\psi_{c_n}) \tag{2.28}$$

then the integral in eq. (2.27) will also factor

$$\mathcal{O}[b] \equiv \int \left(\prod_{n=1}^{N_b} d\psi_{c_n} \right) \mathcal{O}[\psi] = \prod_{n=1}^{N_b} \left(\int d\psi_{c_n} \mathcal{O}_{c_n}(\psi_{c_n}) \right) \tag{2.29}$$

and each integral can be performed separately. To reiterate: to construct an improved estimator of practical value using cluster algorithms, it is necessary that the observable to be averaged can be factored into independent contributions from each cluster.

2.2.4 Solving the Sign Problem

In order to solve the sign problem using a cluster algorithm, two requirements must be satisfied. Firstly, the sign must obey the factoring constraint eq. (2.28). Secondly, the improved estimator must be a sufficient improvement, in that it must uncover enough cancellation in the sense of section 2.2.2. In order to satisfy these requirements, it helps for a model to have a *reference configuration*. A reference configuration is a physical configuration ψ_{ref} which satisfies all cluster configurations and for which $\text{sign}[\psi_{\text{ref}}] = 1$.

Using a cluster algorithm to calculate the integral in eq. (2.25),

$$\int [D\psi]\,\text{sign}[\psi]W[\psi] = \int [Db]\,W[b] \int \left(\prod_{n=1}^{N_b} d\psi_{c_n}\right) \text{sign}[\psi]. \tag{2.30}$$

The first requirement imposes the restriction that for any cluster configuration b

$$\text{sign}[\psi] = \prod_{n=1}^{N_b} \text{sign}_{c_n}(\psi_{c_n}). \tag{2.31}$$

This requirement will be satisfied if a sign can be assigned to each state of each cluster. For the models treated in this thesis, sites and clusters have just two states. If flipping a cluster changes its sign, that cluster shall be called a *meron*[2]. Thus if there are any merons at all, the value of the improved estimator for the sign

$$\text{sign}[b] = \prod_{n=1}^{N_b} \left(\int d\psi_{c_n} \text{sign}_{c_n}(\psi_{c_n}) \right) \tag{2.32}$$

will be zero.

The simplest way to guarantee that the second requirement will be met is to impose the stronger requirement that *all* cancellation be uncovered – i.e. the value of the improved estimator for the sign should never be negative. Given a reference configuration, this stronger requirement can be satisfied. In the reference configuration,

[2]The term *meron* originally denoted a half instanton. In an earlier algorithm, the clusters which could change the sign were associated with half instantons.[11]

for any cluster configuration,

$$\mathrm{sign}[\psi_{\mathrm{ref}}] = \prod_{n=1}^{N_b} \mathrm{sign}_{c_n}(\psi_{c_n\,\mathrm{ref}}) = 1. \tag{2.33}$$

Here $\psi_{c_n\,\mathrm{ref}}$ is that state of the nth cluster which coincides with the global reference configuration. In this state, all the cluster signs may be set to 1. Any other state of these clusters can be reached by flipping some of the clusters; if the sign for such a configuration is negative, then some of the clusters flipped must be merons.

Given an improved estimator with this structure, the sign problem can be solved by incorporating the value of the improved estimator in the integration into the weight factor. Using this modified weight, a Markov walk will avoid not only those configurations for which the magnitude of the observable is small, but also those for which the contribution will eventually cancel out.

Exactly how the value of the improved estimator is incorporated into the Boltzmann weight is not completely determined. If it is used directly, so that the Boltzmann weight of a configuration is set to zero if there are any merons, then a large segment of configuration space is completely avoided. Although the space avoided does not contribute to the integral, in practice it can be detrimental to avoid it completely. Complete avoidance can lead to problems with the ergodicity of a Markov process used in simulation. Because the sectors of configuration space which have merons may obstruct the walk, it may have difficulty moving between configurations which do contribute. For this reason it can be better to reweight configurations so that it is not impossible but merely unlikely that the walk take a step which increases the number of merons. By biasing the walk against the higher meron sectors in this way, one can gain the benefit of the improved importance sampling while still maintaining ergodicity.

Making Measurements

Once the expectation value of the sign can be computed, it is necessary to move on to computing physical quantities. Because the sign dependence appears not only in the

denominator but also in the numerator of eq. (2.23), the integral in the numerator should also be estimated using an improved estimator. Thus one finally computes $\langle \mathcal{O} \rangle$ as

$$\langle \mathcal{O} \rangle = \frac{\langle \mathcal{O}[\psi] \mathrm{sign}[\psi] \rangle_m}{\langle \mathrm{sign}[\psi] \rangle_m} \tag{2.34}$$

$$= \frac{\int [Db]\, W[b] \int \left(\prod_{n=1}^{N_b} d\psi_{c_n} \right) \mathcal{O}[\psi] \mathrm{sign}[\psi]}{\int [Db]\, W[b] \int \left(\prod_{n=1}^{N_b} d\psi_{c_n} \right) \mathrm{sign}[\psi]} \tag{2.35}$$

$$= \frac{\int [Db]\, W[b]\, (\mathcal{O} \cdot \mathrm{sign})\, [b]}{\int [Db]\, W[b] \mathrm{sign}[b]}. \tag{2.36}$$

Here, the inner integrations in eq. (2.35) may be computed explicitly, as they range only over all orientations of given clusters. If the cluster algorithm is sufficiently well constructed, these explicit integrations will average out the dramatic fluctuations of their integrand, and the remaining integrals can be efficiently estimated using importance sampling.

Chapter 3

D-Theory for (1+1+1)D $O(3)$

The $1+1$ dimensional $O(3)$ model shares some properties with QCD such as a mass gap, asymptotic freedom, instantons and theta-vacua. It is also relatively simple and well understood. In fact, the mass gap and the the particle number density as a function of chemical potential can be calculated to very high precision in the infinite volume, zero temperature limit [32, 33]. This model has a D-Theory formulation, in which numerical simulations may easily be performed using cluster algorithms. Like more complex systems, such simulations encounter efficiency problems when a chemical potential is introduced. All these qualities make it a good candidate for experimenting with a solution for the sign problem.

3.1 Defining the System

3.1.1 The Classical Action

The Euclidean action for this system takes the form

$$S[\hat{e}] = \frac{1}{2g^2} \int d^2x \partial_\mu \hat{e} \cdot \partial_\mu \hat{e}, \tag{3.1}$$

which readily exhibits the global $O(3)$ symmetry of the system as it is invariant under $\hat{e}(x) \to R\hat{e}(x)$ for any rotation R. Regularizing this action on a lattice by replacing

the derivatives by finite differences with lattice spacing a, S becomes

$$S[\hat{e}] = \frac{1}{2g^2} \sum_x a^2 \sum_\mu \frac{(\hat{e}_{x+\mu} - \hat{e}_x)}{a} \cdot \frac{(\hat{e}_{x+\mu} - \hat{e}_x)}{a} = \frac{1}{g^2} \sum_{x,\mu} (1 - \hat{e}_x \cdot \hat{e}_{x+\mu}) \,. \tag{3.2}$$

Dropping the irrelevant leading constant, this is simply

$$S[\hat{e}] = -\frac{1}{g^2} \sum_{x,\mu} \hat{e}_x \cdot \hat{e}_{x+\mu}. \tag{3.3}$$

3.1.2 Constructing a Quantized Action

A D-Theory quantized Euclidean action $\mathbb{S}$ may be constructed from S by replacing the components of $\hat{e}_x$ with appropriately chosen operators $\hat{\mathbf{e}}_x$. These operators must be chosen so as to represent the components of unit vectors – i.e. the vector of operators must transform in the adjoint representation of the rotation group, and operators at different sites must commute. For rotation generators $\vec{\mathbb{L}}$, the operators $\hat{\mathbf{e}}_x$ must satisfy

$$\left[\mathbb{L}^i, \mathbf{e}_x^j\right] = i\epsilon^{ijk}\mathbf{e}_x^k \qquad \text{and} \qquad \left[\mathbf{e}_x^i, \mathbf{e}_y^j\right] \propto \delta_{xy}. \tag{3.4}$$

These requirements can, of course, be satisfied with a Pauli spin $\frac{1}{2}$ operator $\vec{\sigma}_x$ on each site, $\vec{\mathbf{e}}_x \equiv \frac{1}{2}\vec{\sigma}_x$ and $\vec{\mathbb{L}} \equiv \sum_x \vec{\mathbb{L}}_x \equiv \sum_x \frac{1}{2}\vec{\sigma}_x$. Thus the quantized action takes the form

$$\mathbb{S} = J \sum_{x,\mu} \hat{\mathbf{e}}_x \cdot \hat{\mathbf{e}}_{x+\mu}. \tag{3.5}$$

Here, one of the imperfections in the analogy depicted in fig. 1-1 comes to the fore. The value of J is *not* determined by the corresponding factor in eq. (3.3). In the classical lattice model, a change in the overall sign can be absorbed in a redefinition on half the sites on the lattice, $\hat{e}_x \to -\hat{e}_x$ for every other x. For the quantized case, this redefinition is no longer acceptable, because the operators $-\mathbf{e}^i$ do not satisfy the same commutation relations as the operators $\mathbf{e}^i$.

The quantization prescription suffices, however, as a guide for constructing candidate quantized systems. By utilizing the formal analogy with quantum statistical mechanics, this candidate can be recognized as a quantum Heisenberg magnet with Hamiltonian operator $\mathbb{H}$ in terms of spins $\vec{\mathbb{S}}_x$:

$$\mathbb{H} = J \sum_{x,\mu} \vec{\mathbb{S}}_x \cdot \vec{\mathbb{S}}_{x+\mu}. \tag{3.6}$$

For $J < 0$ this is a ferromagnet, for $J > 0$ an antiferromagnet.

Even in a finite volume, the ferromagnet has a highly degenerate ground state, and its order parameter is conserved – the (unstaggered) magnetization commutes with the Hamiltonian. Also, the Goldstone bosons have a non-relativistic dispersion relation. For these reasons, although dimensional reduction can occur for this system, the ferromagnetic case is more complicated than necessary.

In contrast, the antiferromagnetic choice is relatively simple. At low temperature, the system exhibits long range Néel order – the order parameter in this case is the staggered magnetization, which does not commute with $\mathbb{H}$. This ordered state breaks the global $O(3)$ symmetry to $O(2)$, and so produces two Goldstone modes – spin-waves or magnons. As long range perturbations around the ground state in the coset space $O(3)/O(2) = S^2$, these magnons are described by a continuum effective Lagrangian for a classical unit vector. This effective action can be shown to be

$$S[\vec{e}] = \int_0^\beta dt \int d^2x \, \frac{\rho_s}{2} \left(\partial_\mu \vec{e} \cdot \partial_\mu \vec{e} + \frac{1}{c^2} \partial_t \vec{e} \cdot \partial_t \vec{e} \right) \tag{3.7}$$

to lowest order [14, 15]. Here ρ_s is the spin stiffness and c is the magnon velocity. This effective system may be considered as a three dimensional classical statistical mechanics problem with finite extent in the third direction. The Goldstone bosons in this theory, being massless in the $\beta \to \infty$ limit, will correspond to very long correlation length excitations at finite β. Thus at least as far as those excitations are concerned, the finite extent of the third direction will be infinitesimal, and so dimensional reduction down to two dimensions will occur in the large β limit. As the

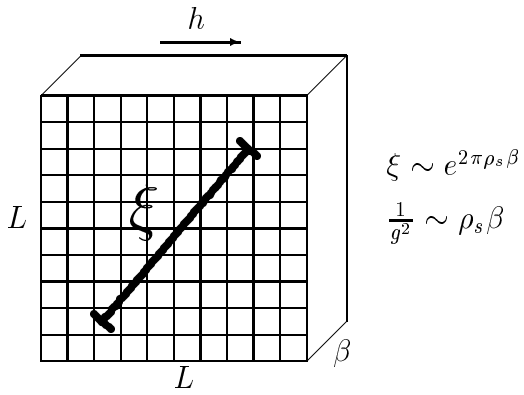

For appropriate choice of β, $\beta c \ll \xi \ll L$.

Figure 3-1: *Dimensional reduction of a* (2+1)*D Heisenberg antiferromagnet to produce a* (1+1)*D* $O(3)$ *quantum field theory.*

correlation length becomes greater than βc, $\vec{e}$ must become essentially independent of t. Thus t can be integrated out of the action:

$$S[\vec{e}] = \int_0^\beta dt \int d^2x \; \frac{\rho_s}{2} \left(\partial_\mu \vec{e} \cdot \partial_\mu \vec{e} + \frac{1}{c^2} \partial_t \vec{e} \cdot \partial_t \vec{e} \right) \tag{3.8}$$

$$\approx \left(\int_0^\beta dt \right) \int d^2x \; \frac{\rho_s}{2} \partial_\mu \vec{e} \cdot \partial_\mu \vec{e} \tag{3.9}$$

$$= \frac{\beta \rho_s}{2} \int d^2x \; \partial_\mu \vec{e} \cdot \partial_\mu \vec{e}. \tag{3.10}$$

The resulting approximate two dimensional action has precisely the form of eq. (3.1) with $\frac{1}{g^2} = \rho_s \beta$. Moreover, the approximation gets better as $\beta \to \infty$ and the t dependence of $\vec{e}$ becomes smaller.

Unlike in the three dimensional system, in the two dimensional system the Goldstone bosons cannot be massless. The Mermin-Wagner-Coleman theorem asserts that massless, non-interacting excitations do not occur in two or fewer dimensions. Essentially, there is not sufficient connectivity between points in a two dimensional space for information to propagate well enough to form infinite correlation length structure. Indeed, the resulting (1+1)D $O(3)$ model is known to have a non-perturbatively generated mass gap.

Using chiral perturbation theory, one can express the coupling constant g of the

resulting 1+1 dimensional theory in terms of the parameters in the 3 dimensional action [33]:

$$\frac{1}{g^2} = \beta\rho_s - \frac{3}{16\pi^2\beta\rho_s} + \mathcal{O}\left(\frac{1}{\beta^2\rho_s^2}\right), \tag{3.11}$$

and can show the mass gap to be [33, 15]

$$m = \frac{16\pi\rho_s}{ec} e^{-2\pi\beta\rho_s}\left[1 + \frac{1}{4\pi\beta\rho_s} + \mathcal{O}\left(\frac{1}{\beta^2\rho_s^2}\right)\right]. \tag{3.12}$$

Thus during the crossover into the dimensionally reduced system as $\beta \to \infty$, the correlation length $\xi \equiv \frac{1}{m}$ grows exponentially with β. This exponential dependence makes it relatively easy to choose a practical β – one not too large for simulation but large enough that $\xi \gg \beta c$ and dimensional reduction occurs.

3.2 Adding Chemical Potential

3.2.1 The Original Continuum

Given an action with a global symmetry, a chemical potential can be introduced as would a constant, imaginary, time-like gauge field. Note that in this one aspect this model is more complicated than QCD: the global symmetry here is $O(3)$ – which is non-Abelian – while in QCD the symmetry of interest is the $U(1)$ of baryon number – which is Abelian. Thus here the chemical potential is a three component vector $\vec{h}$. A normal gauge field would modify the derivative in equation (3.1) as

$$\partial_\mu \hat{e}(x) \to \left(\partial_\mu - iA_\mu^k(x)L_k\right)\hat{e}(x), \tag{3.13}$$

where $A_\mu^k(x)$ is real and the L_k are a hermitian generators of rotations for $\hat{e}$. Since $\hat{e}$ is in the fundamental representation of $O(3)$, this amounts to

$$\partial_\mu \hat{e}(x) \to \partial_\mu \hat{e}(x) - \vec{A}_\mu(x) \times \hat{e}(x), \tag{3.14}$$

in which all factors are real. According to the prescription above, in order to introduce a chemical potential, an imaginary term should be introduced into eq. (3.1) as $A^k_\mu(x) = i\delta_{\mu,1}h^k$, so that

$$\partial_\mu e^i(x) \to \partial_\mu e^i(x) + \delta_{\mu,1}h^k L^{ij}_k e^j(x). \tag{3.15}$$

Thus, the effect of the chemical potential is to rotate spins transported along the first direction (the time-like direction in the $1+1$ dimensional model) by an imaginary angle. In particular,

$$\partial_\mu \hat{e}(x) \to \partial_\mu \hat{e}(x) - i\delta_{\mu,1}\vec{h} \times \hat{e}(x) \tag{3.16}$$

which is *not* real, and so the two dimensional action becomes

$$S[\hat{e}] = \frac{1}{2g^2}\int d^2x \left(\partial_\mu \hat{e} - i\delta_{\mu,1}\vec{h}\times\hat{e}\right)\cdot\left(\partial_\mu \hat{e} - i\delta_{\mu,1}\vec{h}\times\hat{e}\right) \tag{3.17}$$

$$= \frac{1}{2g^2}\int d^2x \left[\partial_\mu\hat{e}\cdot\partial_\mu\hat{e} - 2i\left(\vec{h}\times\hat{e}(x)\right)\cdot\partial_1\hat{e} - \left(\vec{h}\times\hat{e}(x)\right)^2\right]. \tag{3.18}$$

This action is explicitly complex, and so direct simulation of the $1+1$ dimensional $O(3)$ model encounters a complex action problem.

3.2.2 On the D-Theory Lattice

In order to add the chemical potential in the D-Theory formulation, it must be introduced into the lattice action eq. (3.3). The version of eq. (3.15) for the lattice, in terms of finite differences, is

$$\frac{(\hat{e}_{x+\mu} - \hat{e}_x)}{a} \to \frac{\left(R(-i\delta_{\mu,1}ah^k)\hat{e}_{x+\mu} - \hat{e}_x\right),}{a} \tag{3.19}$$

where $R(\vec{n})$ is a rotation operator about axis $\hat{n}$ by angle $|n|$. Since the operators $\vec{\mathbf{e}}$ transform in the adjoint representation, the quantized action in equation (3.5)

becomes

$$\mathbb{S} = J \sum_{x,\mu} \hat{\mathbf{e}}_x \cdot \left[\mathbb{R}(-i\delta_{\mu,1} a h^k) \hat{\mathbf{e}}_{x+\mu} \mathbb{R}^{-1}(-i\delta_{\mu,1} a h^k) \right] \tag{3.20}$$

$$= J \sum_{x,\mu} \hat{\mathbf{e}}_x \cdot \left[\left(e^{-\delta_{\mu,1} a h^k \mathbb{L}^k_{x+\mu}} \right) \hat{\mathbf{e}}_{x+\mu} \left(e^{\delta_{\mu,1} a h^k \mathbb{L}^k_{x+\mu}} \right) \right]. \tag{3.21}$$

Equivalently, in the language of the quantum magnet,

$$\mathbb{H} = J \sum_{x,\mu} \vec{\mathbb{S}}_x \cdot \left[\left(e^{-\delta_{\mu,1} a h^k \mathbb{S}^k_{x+\mu}} \right) \vec{\mathbb{S}}_{x+\mu} \left(e^{\delta_{\mu,1} a h^k \mathbb{S}^k_{x+\mu}} \right) \right]. \tag{3.22}$$

This modification of the Hamiltonian in eq.(3.6) should result in a corresponding modification to the low energy effective action in eq. (3.7):

$$S[\vec{e}] = \int_0^\beta dt \int d^2x \frac{\rho_s}{2} \left[\left(\partial_\mu \hat{e} - i\delta_{\mu,1} \vec{h} \times \hat{e} \right) \cdot \left(\partial_\mu \hat{e} - i\delta_{\mu,1} \vec{h} \times \hat{e} \right) + \frac{1}{c^2} \partial_t \vec{e} \cdot \partial_t \vec{e} \right]. \tag{3.23}$$

In turn, this $2+1$ dimensional effective action should dimensionally reduce as the correlation length becomes larger than β, finally producing

$$S[\vec{e}] = \int_0^\beta dt \int d^2x \ \frac{\rho_s}{2} \left[\left(\partial_\mu \hat{e} - i\delta_{\mu,1} \vec{h} \times \hat{e} \right) \cdot \left(\partial_\mu \hat{e} - i\delta_{\mu,1} \vec{h} \times \hat{e} \right) + \frac{1}{c^2} \partial_t \vec{e} \cdot \partial_t \vec{e} \right] \tag{3.24}$$

$$\approx \left(\int_0^\beta dt \right) \int d^2x \ \frac{\rho_s}{2} \left(\partial_\mu \hat{e} - i\delta_{\mu,1} \vec{h} \times \hat{e} \right) \cdot \left(\partial_\mu \hat{e} - i\delta_{\mu,1} \vec{h} \times \hat{e} \right) \tag{3.25}$$

$$= \frac{\rho_s \beta}{2} \int d^2x \ \left(\partial_\mu \hat{e} - i\delta_{\mu,1} \vec{h} \times \hat{e} \right) \cdot \left(\partial_\mu \hat{e} - i\delta_{\mu,1} \vec{h} \times \hat{e} \right) \tag{3.26}$$

$$\approx \frac{1}{2g^2} \int d^2x \ \left(\partial_\mu \hat{e} - i\delta_{\mu,1} \vec{h} \times \hat{e} \right) \cdot \left(\partial_\mu \hat{e} - i\delta_{\mu,1} \vec{h} \times \hat{e} \right). \tag{3.27}$$

Thus numerical study of the system described by eq. (3.22) can produce results for the target theory described in eq. (3.17).

3.2.3 Known Exact Results

The response of the particle number density to a chemical potential in the (1+1)D $O(3)$ model is known exactly in the limit of zero temperature and infinite volume from

Bethe ansatz techniques [32, 33]. Specifically, when the magnitude of the chemical potential h is larger than the mass gap m, the free energy density f is given by

$$f(h) - f(0) = -\frac{1}{2\pi} \int_{-\theta_0}^{\theta_0} d\theta \epsilon(\theta)\, m \cosh\theta, \tag{3.28}$$

where the function $\epsilon(\theta)$ satisfies the integral equation

$$\epsilon(\theta) - \int_{-\theta_0}^{\theta_0} d\theta' \frac{\epsilon(\theta')}{(\theta' - \theta)^2 + \pi^2} = h - m\cosh\theta, \tag{3.29}$$

and θ_0 is defined by the boundary condition $\epsilon(\pm\theta_0) = 0$. For any fixed θ_0, this equation is an inhomogeneous Fredholm integral equation of the second kind and can be solved for $\epsilon(\theta)$ with standard numerical techniques [39]. The boundary condition on θ_0 can then be enforced simply by searching in θ_0 for the root of $\epsilon(\theta_0)$. For $h < m$, no particles are formed, and so at zero temperature, $f(h) = f(0)$. Once $f(h)$ is known, the particle number density is given by $\frac{df(h)}{dh}$. This result provides a known point of comparison for a numerical study of the particle number density at finite temperature.

When the chemical potential is below the threshold of the mass gap, the solution above predicts no particle density at all, as it is valid only at zero temperature and infinite volume. When the temperature is non-zero and the size of the system is finite, particles will occasionally be created even when the chemical potential is below the mass gap because of thermal fluctuations. At sufficiently low temperatures, the result will be a dilute gas of particles. Although the particles are interacting bosons, in this one dimensional system the behaviors of hard-core bosons and non-interacting fermions are sufficiently similar that the particle number density in the threshold region may be modeled as a simple dilute gas of non-interacting fermions in a box. Without antiparticles, such a model yields the prediction

$$N_p(h) = \frac{1}{L} \sum_{n=0}^{L-1} \left[1 + e^{\beta\left(\sqrt{m^2 + 4\sin^2\frac{n\pi}{L}} - h\right)} \right]^{-1}. \tag{3.30}$$

Antiparticles behave exactly the same way except their response to h is opposite – i.e.

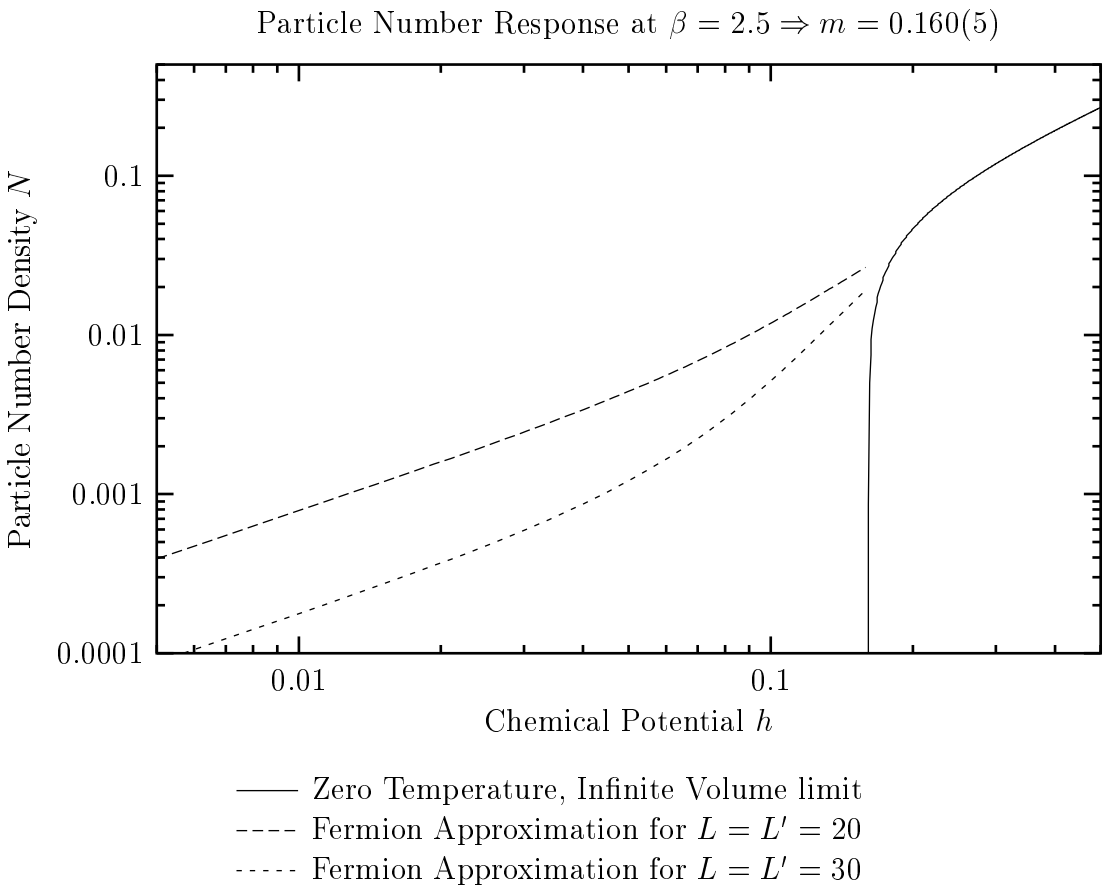

Figure 3-2: *Exact results for the particle number density in* 1+1 *dimensional* $O(3)$ *at* $m = 0.160(5)$. *The solid line is the Bethe ansatz result for the* $L = L' = \infty$ *limit. The upper and lower dashed lines are the dilute fermion gas estimates from eq. (3.31) for* $L = L' = 20$ *and* $L = L' = 30$ *respectively.*

$N_a(h) = N_p(-h)$. Since the fermions are non-interacting, the total particle number density is then

$$N(h) = N_p(h) - N_a(h). \tag{3.31}$$

Both the Bethe ansatz solution and some examples of the fermion gas approximation are shown in fig. 3-2.

Chapter 4

Constructing a Cluster Algorithm for (1+1+1)D $O(3)$

Several steps must be taken to build a cluster algorithm in order to explore the D-Theory representation of the (1+1)D $O(3)$ model. First, the transfer matrix must be calculated from the D-Theory Hamiltonian. Second, the transfer matrix must be analyzed and separated into breakups so as to satisfy eq. (2.14). Third, if any elements of the transfer matrix are negative, the applicability of eq. (2.31) must be verified, and rules must be found to determine the signs of the clusters. Fourth and finally, having constructed an algorithm to estimate the partition function, an improved estimator must be constructed for any observable which is to be measured. The observable of interest here is the particle number density.

Because the chemical potential in this model is coupled to a charge of a non-Abelian symmetry – the global $O(3)$ symmetry – the introduction of the chemical potential breaks the symmetry. It is necessary to choose an axis around which h prefers to rotate the spins. Having thus chosen an axis, there is further a choice: the angle between the quantization axis and the chemical potential. Although this angle has no physical significance, it can dramatically affect the structure of a cluster algorithm constructed from the transfer matrix. When the quantization axis is parallel to the chemical potential, no signs are introduced. Nevertheless, the cluster algorithm becomes inefficient. When the quantization axis is transverse to the chemical poten-

tial, a sign problem develops. The algorithm becomes inefficient, but this inefficiency can now be repaired using merons.

4.1 Without Chemical Potential

The introduction of a chemical potential modifies the Hamiltonian of the system, and in turn modifies the transfer matrix and the structure of the cluster algorithm. As a point of reference, consider first the system without chemical potential. For the sake of consistency, the language of statistical mechanics shall be used henceforth, describing the system in terms of a Hamiltonian $\mathbb{H}$.

4.1.1 The Transfer Matrix

The Hamiltonian for the antiferromagnet is shown in eq. (3.6) as

$$\mathbb{H} = J \sum_{x,\mu} \vec{\mathbb{S}}_x \cdot \vec{\mathbb{S}}_{x+\mu}, \tag{4.1}$$

where $J > 0$. From eq. (2.5), the transfer matrix is then

$$\mathbb{T} = e^{-\epsilon J \vec{\mathbb{S}}_x \cdot \vec{\mathbb{S}}_{x+\mu}}. \tag{4.2}$$

Writing the vector product in index notation, suppressing the spatial indices, and using the order across the tensor product $\otimes$ to keep track of the difference between x and $x + \mu$, this is

$$\mathbb{T} = e^{-\epsilon J \mathbb{S}_i \otimes \mathbb{S}_i}. \tag{4.3}$$

This object has four indices, one for the spin at each corner of a plaquette, each of which takes on two values, $\uparrow$ and $\downarrow$. By convention, $\uparrow$ shall always come before $\downarrow$. In order to write this matrix out, it is necessary to pair up its indices in order to bring the number of indices down enough to fit onto a two dimensional sheet of

paper. Again by convention, whenever two indices are paired, the latter index shall vary fastest – the order shall be $\uparrow\uparrow, \uparrow\downarrow, \downarrow\uparrow, \downarrow\downarrow$. For the moment, the indices shall be paired for time-like multiplication, as in eq. (2.8).

In this basis, the transfer matrix is

$$\begin{aligned}
\mathbb{T} &= e^{-\frac{\epsilon J}{4}\sigma^i\otimes\sigma^i} \\
&= e^{-\frac{\epsilon J}{4}\left(\begin{bmatrix} 0&0&0&1\\0&0&1&0\\0&1&0&0\\1&0&0&0\end{bmatrix}+\begin{bmatrix} 0&0&0&-1\\0&0&1&0\\0&1&0&0\\-1&0&0&0\end{bmatrix}+\begin{bmatrix} 1&0&0&0\\0&-1&0&0\\0&0&-1&0\\0&0&0&1\end{bmatrix}\right)} \\
&= e^{-\frac{\epsilon J}{4}\left(\mathbb{I}+\begin{bmatrix} 0&0&0&0\\0&-2&2&0\\0&2&-2&0\\0&0&0&0\end{bmatrix}\right)} \\
&= e^{\frac{\epsilon J}{4}}\left(\mathbb{I}e^{-\frac{\epsilon J}{2}}+\sinh\frac{\epsilon J}{2}\begin{bmatrix} 0&0&0&0\\0&1&-1&0\\0&-1&1&0\\0&0&0&0\end{bmatrix}\right).
\end{aligned} \tag{4.4}$$

The overall multiplicative factor can be absorbed in the normalization of the partition function, and so will be discarded. Expanding to first order in ϵ, the transfer matrix becomes

$$\mathbb{T} \approx \left(1-\frac{\epsilon J}{2}\right)\begin{bmatrix} 1&0&0&0\\0&1&0&0\\0&0&1&0\\0&0&0&1\end{bmatrix}+\frac{\epsilon J}{2}\begin{bmatrix} 0&0&0&0\\0&1&-1&0\\0&-1&1&0\\0&0&0&0\end{bmatrix} \tag{4.5}$$

$$= \begin{bmatrix} 1-\frac{\epsilon J}{2}&0&0&0\\0&1&-\frac{\epsilon J}{2}&0\\0&-\frac{\epsilon J}{2}&1&0\\0&0&0&1-\frac{\epsilon J}{2}\end{bmatrix}. \tag{4.6}$$

The negative signs in this matrix may at first seem disturbing, as there should not be a sign problem in this case with no chemical potential – no terms in the partition function integral should be negative. These signs will cancel out. They are off diagonal in $\mathbb{T}$, and hence they are associated with *transitions*[1]. It is not possible to have a configuration on the lattice with an odd number of transitions on a periodic

[1] instances where a spin changes state between time slices

lattice with even spatial extents.

4.1.2 Breakups

Equation (4.5) is of the form

$$\mathbb{T} = \sum_{b=1}^{n_b} w_b \mathbb{B}_b \,, \tag{4.7}$$

where in this case $n_b = 2$. The two matrices $\mathbb{B}_1$ and $\mathbb{B}_2$ have entries which are all of magnitude either one or zero. They can be interpreted as constraints upon the spins at the four corners of the plaquette on which $\mathbb{T}$ is acting – i.e. breakups. To each breakup $\mathbb{B}_b$ is assigned a corresponding weight w_b.

The first matrix, $\mathbb{B}_1$, is the identity. It represents the constraint "no spin shall change as it propagates in the third direction". It is non-zero only for four configurations. It corresponds to a pattern of bonds – two bonds connecting the spins constrained to be the same – those paired vertically, and so shall be called the *vertical breakup*.

The second matrix, $\mathbb{B}_2$, represents the constraint "each spin shall be the opposite of its sideways partner". It also is non-zero only for four configurations. It corresponds to a pattern of bonds connecting the spins constrained to be different – this time they are paired horizontally, and so $\mathbb{B}_2$ shall be called the *horizontal breakup*.

Note that the spin configurations allowed for these two breakups are the only configurations for which the Boltzmann weight is not zero. These two breakups and their respective allowed spins are depicted in table 4.1. If the spins on a given plaquette satisfy the vertical breakup, the state of that plaquette is called a *continuation*. If they do not, so that only the horizontal breakup applies, the state a transition.

Expanding an entire integral of the form of eq. (2.12) using this decomposition of $\mathbb{T}$, and using the global cancellation of the signs to justify ignoring them,

$$\int [D\psi]\, \mathcal{O}[\psi] \prod_{t,\mu,x} T_{t,\mu,x} = \int [D\psi]\, \mathcal{O}[\psi] \left| \prod_{t,\mu,x} T_{t,\mu,x} \right| \tag{4.8}$$

$$= \int [D\psi]\, \mathcal{O}[\psi] \prod_{t,\mu,x} |T_{t,\mu,x}| \tag{4.9}$$

$$= \int [D\psi]\, \mathcal{O}[\psi] \prod_{t,\mu,x} \left| \sum_{b_{t,\mu,x}=1}^{n_b} w_{n_{t,\mu,x}} B_{b_{t,\mu,x}} \right|. \tag{4.10}$$

Because there are no cancellations in eq. (4.7), it is

$$= \int [D\psi]\, \mathcal{O}[\psi] \prod_{t,\mu,x} \left[\sum_{b_{t,\mu,x}=1}^{n_b} w_{n_{t,\mu,x}} \left| B_{b_{t,\mu,x}} \right| \right]. \tag{4.11}$$

Rewriting the many small sums as one big path integral, the integral is

$$= \int [D\psi] \int [Db]\, \mathcal{O}[\psi] \prod_{t,\mu,x} w_{b_{t,\mu,x}} \left| B_{b_{t,\mu,x}} \right| \tag{4.12}$$

$$= \int [D\psi]\, [Db]\, \mathcal{O}[\psi] \left(\prod_{t,\mu,x} w_{b_{t,\mu,x}} \right) \left(\prod_{t,\mu,x} \left| B_{b_{t,\mu,x}} \right| \right) \tag{4.13}$$

$$\equiv \int [D\psi]\, [Db]\, \mathcal{O}[\psi] W[b] \delta[\psi, b] \tag{4.14}$$

$$= \int [Db]\, W[b] \int \left(\prod_{n=1}^{N_b} d\psi_{c_n} \right) \mathcal{O}[\psi]. \tag{4.15}$$

which, finally, reproduces the structure promised in section 2.1.4 and in eq. (2.19).

To put this representation into use, a Markov walk is used to generate an ensemble for the joint distribution of breakups and spins determined by $W[\psi, b] = W[b]\delta[\psi, b]$. For any spin configuration there is a fixed set of breakups with non-zero weight. Given a spin configuration on the lattice, breakups are chosen for each plaquette randomly, according to their relative weight among the acceptable possibilities. The relevant information is summarized in table 4.2. For example, given the spin configuration on the second row of the table, the vertical breakup would be chosen with probability $(1 - \frac{\epsilon J}{2})/1$, while the horizontal breakup would be chosen with probability $(\frac{\epsilon J}{2})/1$. Given the configuration on the third row, the horizontal breakup would be chosen with probability $(\frac{\epsilon J}{2})/(\frac{\epsilon J}{2}) = 1$. A typical joint configuration for a 1+1 dimensional system is shown in fig. 4-1.

Matrix	Diagram	Allowed configurations
$\mathbb{B}_1 = \begin{bmatrix} 1 & 0 & 0 & 0 \\ 0 & 1 & 0 & 0 \\ 0 & 0 & 1 & 0 \\ 0 & 0 & 0 & 1 \end{bmatrix}$		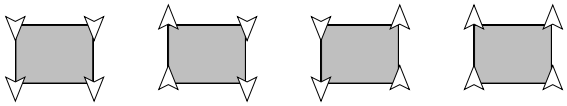
$\mathbb{B}_2 = \begin{bmatrix} 0 & 0 & 0 & 0 \\ 0 & 1 & -1 & 0 \\ 0 & -1 & 1 & 0 \\ 0 & 0 & 0 & 0 \end{bmatrix}$		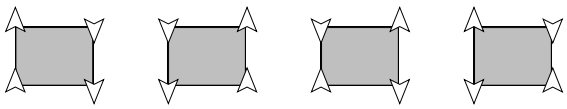

Table 4.1: *The vertical and horizontal breakups for* (1+1+1)*D* $O(3)$ *and the spin configurations which satisfy them. The horizontal bonds are cross-hatched (▭) to indicate that the sign contributed by the plaquette changes when the spins on the bond are flipped.*

Typical Spins	Total Weight	 $1 - \frac{\epsilon J}{2}$	 $\frac{\epsilon J}{2}$
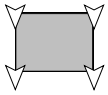	$1 - \frac{\epsilon J}{2}$	$+$	
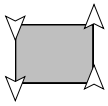	1	$+$	$+$
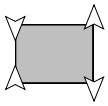	$-\frac{\epsilon J}{2}$		$-$

Table 4.2: *The assignment of weights to the breakups for* (1+1+1)*D* $O(3)$ *with no chemical potential. In each row, the weights of the breakups selected, multiplied by the indicated signs, add up to the total weight for the row. In each column, only spin configurations allowed for the breakup are selected, and the sign corresponds to whether the bonds flipped relative to the staggered reference configuration is cross-hatched (▭).*

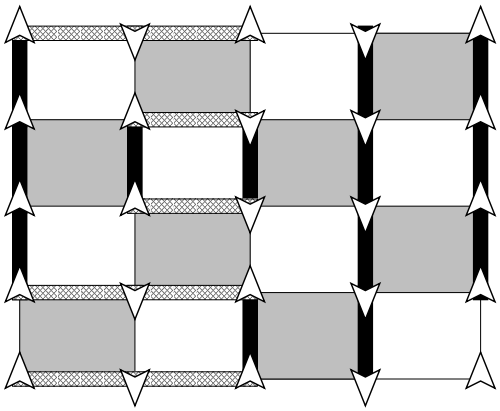

Figure 4-1: *A typical joint configuration of spins and clusters for a* 1+1 *dimensional Heisenberg antiferromagnet cluster algorithm. The grey squares are those on which the transfer matrix acts, while white squares are empty space imposed by the Trotter decomposition. Thus this lattice is only* 2ϵ *high. Only the small square loop in the middle is oriented against the reference configuration.*

4.1.3 The Canceling of the Minus Signs

A minus sign must be included for every transition plaquette. In fact, although there will be no configurations with minus signs in the end, proving as much is an excellent task for a first application of the meron concept. To attribute these signs to clusters, it will help to find a reference configuration. This system has two potential reference configurations – those in which the spins are completely staggered in the spatial directions, but aligned with their neighbors in the third direction.

Consider choosing one of the two possibilities as reference configuration. Transitions always occur along with horizontal breakups. Moreover, the two bonds in the horizontal breakup must be aligned differently for there to be a transition. Thus if $N_{h,a}$ is the number of horizontal bonds which are oriented against the reference configuration, the sign is $(-1)^{N_{h,a}}$. By collecting all the signs from horizontal bonds in a given cluster, each cluster can be assigned a sign. If a cluster is oriented against the reference configuration and it has an odd number of horizontal bonds, then it will produce a minus sign. The global sign is then the product of the cluster signs, in accordance with eq. (2.31).

A cluster is hence a meron precisely when it has an odd number of horizontal segments. However, careful inspection of the possible cluster shapes will reveal – for this simple case with no chemical potential – that clusters must have an even number of horizontal segments. The clusters are loops, and they step horizontally at the same times that they turn around in the third direction. In order to close, a loop must turn around an even number of times, hence it must step horizontally an even number of times. Thus one can see that the signs which appear on individual plaquettes as recorded in eq. (4.6) cancel out once the whole lattice is taken into account.

4.1.4 The Operation of the Cluster Algorithm

Starting from a physical configuration, the cluster algorithm generates a Markov step by tiling the lattice with randomly chosen breakups as described above, and then choosing at random a new orientation for each cluster. The orientations for the clusters are easy to choose because – by construction – the Boltzmann factor contributed by each plaquette for a fixed breakup is independent of the physical state, in accordance with eq. (2.19). In other words, once the cluster configuration is chosen, any one set of cluster orientations has precisely the same Boltzmann weight as any other.

When implementing this algorithm, it is not actually necessary to record the spins on the lattice at all. They can always be inferred from the cluster configuration and orientations. Instead of wiping the lattice clean of cluster configurations and starting fresh, it is sufficient to break up such a large update into many smaller (and proportionally faster) updates. One can pick a plaquette at random, choose at random an orientation for all clusters touching that plaquette to determine its spins, and given the spins choose a new breakup. Thus the joint configuration can be updated without actually keeping any permanent record of the spins across the lattice at all.

4.2 Adding the Chemical Potential

Having constructed a cluster algorithm for the simple case with no chemical potential, one can now proceed to introduce the chemical potential and see what changes are necessary. The Hamiltonian now takes the form given in eq. (3.22):

$$\mathbb{H} = J \sum_{x,\mu} \vec{\mathbb{S}}_x \cdot \left[\left(e^{-\delta_{\mu,1} a h^k \mathbb{S}^k_{x+\mu}} \right) \vec{\mathbb{S}}_{x+\mu} \left(e^{\delta_{\mu,1} a h^k \mathbb{S}^k_{x+\mu}} \right) \right]. \tag{4.16}$$

Because the rotation operators at x commute with the spin operators at $y \neq x$, they can be taken down out of the exponent defining the transfer matrix, and eq. (4.4) becomes

$$\mathbb{T} = \left(e^{\delta_{\mu,1} \vec{h} \cdot \vec{\mathbb{S}}_{x+\mu}} \right) e^{-\epsilon J \vec{\mathbb{S}}_x \cdot \vec{\mathbb{S}}_{x+\mu}} \left(e^{-\delta_{\mu,1} \vec{h} \cdot \vec{\mathbb{S}}_{x+\mu}} \right) \tag{4.17}$$

$$= e^{\delta_{\mu,1} h^i \cdot \left(\mathbb{I} \otimes \frac{\sigma^i}{2} \right)} e^{-\frac{\epsilon J}{4} \sigma_i \otimes \sigma_i} e^{-\delta_{\mu,1} h^i \cdot \left(\mathbb{I} \otimes \frac{\sigma^i}{2} \right)} \tag{4.18}$$

$$\propto e^{-\frac{\epsilon J}{2}} + \sinh \frac{\epsilon J}{2} \left(e^{\delta_{\mu,1} h^i \cdot \left(\mathbb{I} \otimes \frac{\sigma^i}{2} \right)} \begin{bmatrix} 0 & 0 & 0 & 0 \\ 0 & 1 & -1 & 0 \\ 0 & -1 & 1 & 0 \\ 0 & 0 & 0 & 0 \end{bmatrix} e^{-\delta_{\mu,1} h^i \cdot \left(\mathbb{I} \otimes \frac{\sigma^i}{2} \right)} \right). \tag{4.19}$$

The rotation operators can be expanded

$$e^{h^i_\mu \cdot \left(\mathbb{I} \otimes \frac{\sigma^i}{2} \right)} = \mathbb{I} \otimes \left[\mathbb{I} \cosh \left(\delta_{\mu,1} \frac{h}{2} \right) + \left(\delta_{\mu,1} \hat{h} \cdot \vec{\sigma} \right) \sinh \left(\delta_{\mu,1} \frac{h}{2} \right) \right] \tag{4.20}$$

$$\equiv \mathbb{I} \otimes \left[c_\mu \mathbb{I} + s_\mu \left(\delta_{\mu,1} \hat{h} \cdot \vec{\sigma} \right) \right] \tag{4.21}$$

where c_μ and s_μ have been defined as

$$c_\mu \equiv \cosh \left(\delta_{\mu,1} \frac{h}{2} \right) \qquad\qquad s_\mu \equiv \sinh \left(\delta_{\mu,1} \frac{h}{2} \right). \tag{4.22}$$

The term in parentheses in eq. (4.19) is then

$$\begin{aligned}\mathbb{I}\otimes\left[c_\mu\mathbb{I}+s_\mu\left(\delta_{\mu,1}\hat{h}\cdot\vec{\sigma}\right)\right]&\\ \cdot\left(\left[\begin{smallmatrix}1&0\\0&0\end{smallmatrix}\right]\otimes\left[\begin{smallmatrix}0&0\\0&1\end{smallmatrix}\right]-\left[\begin{smallmatrix}0&1\\0&0\end{smallmatrix}\right]\otimes\left[\begin{smallmatrix}0&0\\1&0\end{smallmatrix}\right]-\left[\begin{smallmatrix}0&0\\1&0\end{smallmatrix}\right]\otimes\left[\begin{smallmatrix}0&1\\0&0\end{smallmatrix}\right]+\left[\begin{smallmatrix}0&0\\0&1\end{smallmatrix}\right]\otimes\left[\begin{smallmatrix}1&0\\0&0\end{smallmatrix}\right]\right)&\\ \cdot\,\mathbb{I}\otimes\left[c_\mu\mathbb{I}-s_\mu\left(\delta_{\mu,1}\hat{h}\cdot\vec{\sigma}\right)\right]&\end{aligned}\tag{4.23}$$

Rather than proceeding in generality from here, it will be simpler now to choose the relative orientation between $\vec{h}$ and the quantization axis. Two simple choices present themselves: quantize either parallel to or perpendicular to $\vec{h}$.

4.3 Quantize Parallel to the Chemical Potential

4.3.1 The Basic Construction

Choosing $\vec{h}\cdot\vec{\sigma}$ to be $h\sigma_3$, the exponential in eq. (4.21) is[2]

$$\mathbb{I}\otimes\left(c_\mu\mathbb{I}+s_\mu\begin{bmatrix}1&0\\0&-1\end{bmatrix}\right)=\mathbb{I}\otimes\begin{bmatrix}a_\mu&0\\0&b_\mu\end{bmatrix}\tag{4.24}$$

where $a_\mu\equiv e^{\delta_{\mu,1}\frac{h}{2}}$ and $b_\mu\equiv e^{-\delta_{\mu,1}\frac{h}{2}}$. Now (4.23) becomes

$$\begin{aligned}&\left[\begin{smallmatrix}1&0\\0&0\end{smallmatrix}\right]\otimes\left[\begin{smallmatrix}0&0\\0&1\end{smallmatrix}\right]-\left[\begin{smallmatrix}0&1\\0&0\end{smallmatrix}\right]\otimes\left[\begin{smallmatrix}0&0\\b_\mu^2&0\end{smallmatrix}\right]-\left[\begin{smallmatrix}0&0\\1&0\end{smallmatrix}\right]\otimes\left[\begin{smallmatrix}0&a_\mu^2\\0&0\end{smallmatrix}\right]+\left[\begin{smallmatrix}0&0\\0&1\end{smallmatrix}\right]\otimes\left[\begin{smallmatrix}1&0\\0&0\end{smallmatrix}\right]\\ &\qquad=\begin{bmatrix}0&0&0&0\\0&1&-b_\mu^2&0\\0&-a_\mu^2&1&0\\0&0&0&0\end{bmatrix}\end{aligned}\tag{4.25}$$

and, again discarding the irrelevant multiplicative constant, the full transfer matrix for a plaquette along the direction μ is now

$$\mathbb{T}_\mu\propto\mathbb{I}e^{-\frac{\epsilon J}{2}}+\sinh\frac{\epsilon J}{2}\begin{bmatrix}0&0&0&0\\0&1&-b_\mu^2&0\\0&-a_\mu^2&1&0\\0&0&0&0\end{bmatrix}.\tag{4.26}$$

[2] W.l.o.g., h can be taken to be positive. Negative h amounts to the same thing as reflecting the lattice.

Expanding $\mathbb{T}_\mu$ to first order in ϵ, the matrix analogous to eq. (4.6) is

$$\mathbb{T}_\mu \approx \left(1 - \frac{\epsilon J}{2}\right) \begin{bmatrix} 1 & 0 & 0 & 0 \\ 0 & 1 & 0 & 0 \\ 0 & 0 & 1 & 0 \\ 0 & 0 & 0 & 1 \end{bmatrix} + \frac{\epsilon J}{2} \begin{bmatrix} 0 & 0 & 0 & 0 \\ 0 & 1 & -b_\mu^2 & 0 \\ 0 & -a_\mu^2 & 1 & 0 \\ 0 & 0 & 0 & 0 \end{bmatrix} \tag{4.27}$$

$$= \begin{bmatrix} 1 - \frac{\epsilon J}{2} & 0 & 0 & 0 \\ 0 & 1 & -\frac{\epsilon J}{2} b_\mu^2 & 0 \\ 0 & -\frac{\epsilon J}{2} a_\mu^2 & 1 & 0 \\ 0 & 0 & 0 & 1 - \frac{\epsilon J}{2} \end{bmatrix}. \tag{4.28}$$

$\mathbb{T}_\mu$ is, predictably, unchanged when $\mu \neq 1$. However, when $\mu = 1$ the matrix which corresponds to the horizontal breakup has been modified by the introduction of the chemical potential. Now, its elements are no longer all of magnitude 1, which means it is not compatible with the δ-function structure of eq. (2.14).

4.3.2 Adding a Metropolis Step

In order to continue, it is necessary to sacrifice some of the purity of the cluster algorithm – the a^2 and b^2 factors must be included in the inner integral of eq. (2.19). That equation becomes

$$\int [Db] W[b] \int \left(\prod_{n=1}^{N_b} d\psi_{c_n} W[\psi_{c_n}] \right) O[\psi]. \tag{4.29}$$

where $W[\psi_{c_n}]$ will encode the a^2 and b^2 factors. Thus some importance sampling work will remain after the implementation of the cluster algorithm – some cluster orientations will be more important than others. In order to implement this part of the importance sampling, it will be necessary to add a Metropolis step, accepting or rejecting flips of clusters. The need for this accept/reject step bodes ill for the success of this implementation.

Presuming that the a^2 and b^2 factors will thus not be handled by the breakups but elsewhere instead, the breakups for this algorithm are the same as for the case with no chemical potential. As the clusters are still closed loops and the minus signs occur in the same places in the transfer matrix, the argument that the signs cancel

Plaquette State	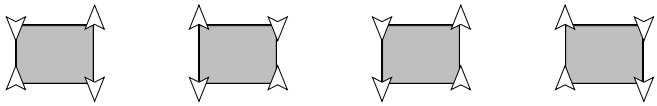			
Metropolis Weight	e^{-h}	e^{h}	1	1

Table 4.3: *Metropolis weights for states of the horizontal breakup in* (1+1+1)*D* $O(3)$ *with quantization axis along the chemical potential*

out which worked in the $h = 0$ case still holds. There is no sign problem.

In order to understand how the a^2 and b^2 factors must enter $W[\psi_{c_n}]$ the algorithm, consider the plaquette states which they affect: the transitions, which are listed in table 4.3. The weights can be attributed to factors from each bond: on the top bond, a factor of $e^{-\frac{h}{2}}$ for $\uparrow\downarrow$, and a factor of $e^{\frac{h}{2}}$ for $\downarrow\uparrow$; on the bottom bond, the reverse. A simplified picture, in 1+1 dimensions, is given in fig. 4-2. These rules conspire to measure a winding number of clusters. Any cluster which does not wind around the first direction contributes a cumulative factor of 1. Clusters which do wind contribute according to their winding by factors of $e^{L\frac{h}{2}}$, where L is the size of the lattice in the first direction.

In order to update a configuration with this new algorithm, the lattice is tiled with breakups as before, but when clusters are to be flipped, the effect of the cluster winding must be considered. If, for instance, a given cluster winds once around the lattice, then one of its states is more weighty than the other by a factor of e^{Lh}, and its should only be flipped accordingly.

4.3.3 Measuring the Particle Number Density

Now that an algorithm to estimate the partition function has been built, it is necessary to construct an improved estimator for the particle number. It is not immediately apparent what property of the Heisenberg antiferromagnet corresponds to the particle

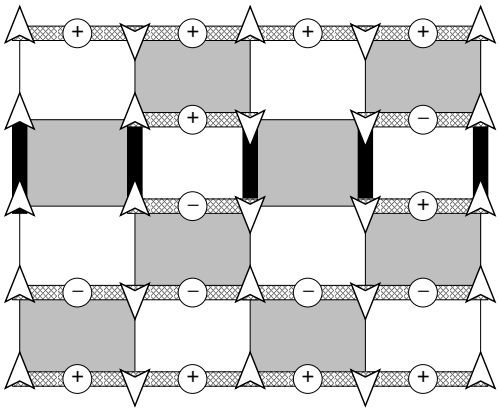

Figure 4-2: *Signs indicating the contribution to the Metropolis weight from each horizontal segment of each cluster. The signs for clusters which do not wind cancel out, whereas for clusters which wind, they add up.*

number of the (1+1)D model. Before an improved estimator can be constructed, the quantity to measure must be identified, and it must be expressed in the language of eq. (2.10). Once that is accomplished, an improved estimator may be constructed by integrating over cluster orientations as in eq. (4.29).

Finding What to Measure

Formally, the particle number density is given by

$$\langle N \rangle \equiv \frac{1}{L}\frac{\partial}{\partial h} \ln Z = \frac{1}{LZ}\frac{\partial}{\partial h} Z. \tag{4.30}$$

Expanding in terms of eqs. (2.7) and (4.9),

$$\langle N \rangle = \frac{1}{LZ}\frac{\partial}{\partial h} \int [D\psi] \prod_{t,\mu,x} |T_{t,\mu,x}| \tag{4.31}$$

$$= \frac{1}{LZ} \int [D\psi] \frac{\partial}{\partial h} \prod_{t,\mu,x} |T_{t,\mu,x}| \tag{4.32}$$

$$= \frac{1}{LZ} \int [D\psi] \left[\sum_{t,\mu,x} \left(\prod_{t',\mu',x' \neq t,x,\mu} |T_{t',\mu',x'}| \right) \frac{\partial}{\partial h} |T_{t,\mu,x}| \right]. \tag{4.33}$$

The ensemble generated to estimate Z is determined by the weight

$$W[\psi] = \prod_{t,\mu,x} |T_{t,\mu,x}|. \tag{4.34}$$

In order to continue to use the same ensemble it is desirable to write eq. (4.33) in terms of the same weight. Thus consider[3]

$$\langle N \rangle = \frac{1}{LZ} \int [D\psi] \left(\prod_{t,\mu,x} |T_{t,\mu,x}| \right) \left(\sum_{t',\mu',x'} |T_{t',\mu',x'}|^{-1} \frac{\partial}{\partial h} |T_{t',\mu',x'}| \right). \tag{4.35}$$

Calculating the derivative in the non-trivial case (when $\mu = 1$),

$$\frac{\partial}{\partial h} \begin{bmatrix} 1-\frac{\epsilon J}{2} & 0 & 0 & 0 \\ 0 & 1 & \frac{\epsilon J}{2} e^{-h} & 0 \\ 0 & \frac{\epsilon J}{2} e^{h} & 1 & 0 \\ 0 & 0 & 0 & 1-\frac{\epsilon J}{2} \end{bmatrix} = \begin{bmatrix} 0 & 0 & 0 & 0 \\ 0 & 0 & -\frac{\epsilon J}{2} e^{-h} & 0 \\ 0 & \frac{\epsilon J}{2} e^{h} & 0 & 0 \\ 0 & 0 & 0 & 0 \end{bmatrix}. \tag{4.36}$$

Thus, performing the element-by-element division of eq. (4.35), the quantity to be evaluated on each plaquette is

$$\begin{bmatrix} 0 & 0 & 0 & 0 \\ 0 & 0 & -1 & 0 \\ 0 & 1 & 0 & 0 \\ 0 & 0 & 0 & 0 \end{bmatrix}. \tag{4.37}$$

For each transition where $\downarrow\uparrow$ becomes $\uparrow\downarrow$ the observable measures a -1, while for every transition of the opposite type it measures a 1.

This result may be derived by another more complicated method which will be useful later as a point of comparison. The product in eq.(4.33) lacks a single factor of T. Previously, the missing factor was replaced separately for each physical state ψ, which resulted in the element-by-element division above. Consider instead fixing the product for all states of the plaquette at t, μ, x at once.

Recall that the factors of T in the path integral arise from plaquette operators $\mathbb{T}$. The result of the differentiation is to replace one operator $\mathbb{T}$ with a different

[3]remember $\mathbb{T}$ is a matrix, but T is an element thereof – just a number

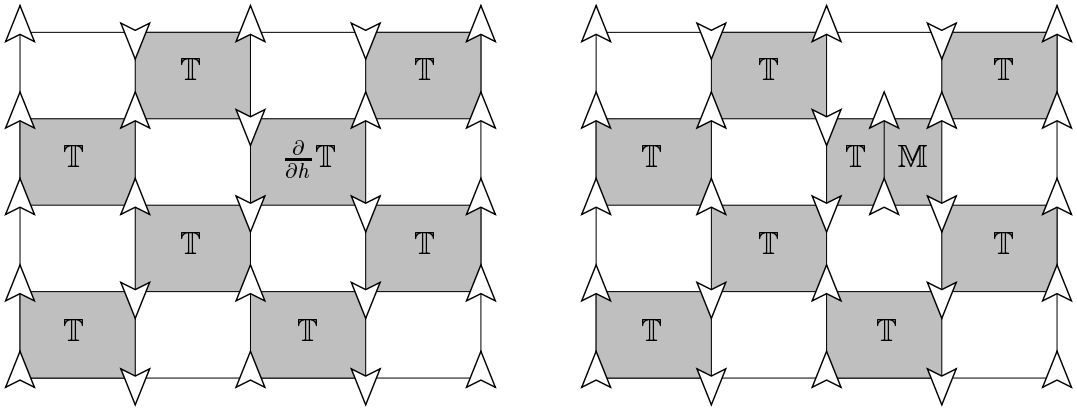

Figure 4-3: *An extra operator* $\mathbb{M}$*, inserted into a* $(1+1)D$ *lattice, to reproduce the effect of changing one transfer matrix. Note that two extra spins are required.*

operator $\frac{\partial}{\partial h}\mathbb{T}$:

$$\frac{\partial}{\partial h}T_{t,\mu,x} = \langle\psi_{t',\mu',x}|\langle\psi_{t',\mu',x+\mu}|\frac{\partial}{\partial h}\mathbb{T}_{t,\mu,x}|\psi_{t,\mu,x}\rangle|\psi_{t,\mu,x+\mu}\rangle. \tag{4.38}$$

If the same result could be obtained not by replacing an operator, but by inserting one, then – at least for some inserted operators, the product could again be repaired. Remember now that the chemical potential is acting in a direction transverse to that in which the Hamiltonian acts. Thus it would be natural to insert an operator not above or below $\mathbb{T}$ but beside it. A typical such replacement is depicted in fig. 4-3.

Plaquette operators acting successively left to right must be multiplied differently than operators acting bottom to top – their components must be arranged with respect to a different sense of "later", using the space-like multiplication $\star$. Such an insertion requires summing over two additional spins – i.e. if $\mathbb{M}$ is the operator which

shall be inserted, it must satisfy[4]

$$\frac{\partial}{\partial h}\mathbb{T}_{t,\mu,x} = \int d\psi'_{t',\mu',x+\mu} d\psi'_{t',\mu'+\mu} \mathbb{M}_{t,\mu,x} \left|\psi'_{t',\mu',x+\mu}\right\rangle \left|\psi'_{t,\mu,x+\mu}\right\rangle \left\langle\psi'_{t',\mu',x+\mu}\right| \left\langle\psi'_{t,\mu,x+\mu}\right| \mathbb{T}_{t,\mu,x} \equiv \mathbb{M}_{t,\mu,x} \star \mathbb{T}_{t,\mu,x}. \quad (4.39)$$

If $\mathbb{M}$, when written for the $\star$ multiplication, happens to be diagonal then the two spins inserted will be redundant. It would be possible to evaluate the result of inserting $\mathbb{M}$ using the configurations already generated, because then it would happen that

$$\mathbb{M}_{t,\mu,x} \left|\psi'_{t',\mu',x+\mu}\right\rangle \left|\psi'_{t,\mu,x+\mu}\right\rangle \left\langle\psi'_{t',\mu',x+\mu}\right| \left\langle\psi'_{t,\mu,x+\mu}\right| = \left|\psi'_{t',\mu',x+\mu}\right\rangle \left|\psi'_{t,\mu,x+\mu}\right\rangle M_{t,\mu,x} \left\langle\psi'_{t',\mu',x+\mu}\right| \left\langle\psi'_{t,\mu,x+\mu}\right| \quad (4.40)$$

in which case

$$\frac{\partial}{\partial h} T_{t,\mu,x} = \langle\psi_{t',\mu',x}| \langle\psi_{t',\mu',x+\mu}| \frac{\partial}{\partial h} \mathbb{T}_{t,\mu,x} |\psi_{t,\mu,x}\rangle |\psi_{t,\mu,x+\mu}\rangle \quad (4.41)$$

$$= M_{t,\mu,x} T_{t,\mu,x}. \quad (4.42)$$

This situation with diagonal $\mathbb{M}$ is depicted in fig. 4-4.

In order to find $\mathbb{M}$, it is necessary to express $\mathbb{T}$ as a four by four matrix with its elements ordered not for the normal time-like multiplication, but for $\star$, the space-like

[4]The order of $\mathbb{T}$ and $\mathbb{M}$ here is a matter of convention – it corresponds to whether one chooses $\mathbb{M}$ to be inserted on the left or on the right of $\mathbb{T}$.

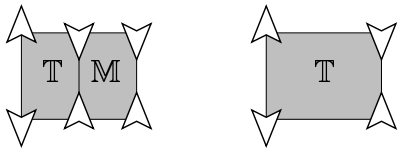

Figure 4-4: *Computing an observable with diagonal* $\mathbb{M}$. *Because* $\mathbb{M}$ *is diagonal, the middle two spins in the diagram on the left drop out, producing the diagram on the right. A factor remains, determined by the state of the rightmost two spins. Here the state of the* $\mathbb{T}$ *plaquette is a transition, and the* $\mathbb{M}$ *produces a* 1.

multiplication. This amounts simply to rearranging the components thus:

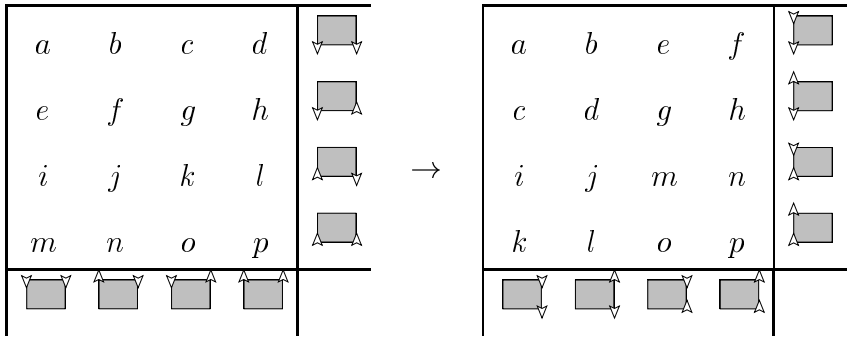

(4.43)

Under this rearrangement, the transfer matrix $\mathbb{T}_1$ from eq. (4.28) changes as follows:

$$\mathbb{T}_1 = \begin{bmatrix} 1-\frac{\epsilon J}{2} & 0 & 0 & 0 \\ 0 & 1 & -\frac{\epsilon J}{2}b_1^2 & 0 \\ 0 & -\frac{\epsilon J}{2}a_1^2 & 1 & 0 \\ 0 & 0 & 0 & 1-\frac{\epsilon J}{2} \end{bmatrix} \tag{4.44}$$

$$= \begin{bmatrix} 1 & 0 & 0 & 0 \\ 0 & 1 & 0 & 0 \\ 0 & 0 & 1 & 0 \\ 0 & 0 & 0 & 1 \end{bmatrix} - \frac{\epsilon J}{2} \begin{bmatrix} 1 & 0 & 0 & 0 \\ 0 & 0 & e^{-h} & 0 \\ 0 & e^{h} & 0 & 0 \\ 0 & 0 & 0 & 1 \end{bmatrix} \tag{4.45}$$

$$\longrightarrow \begin{bmatrix} 1 & 0 & 0 & 1 \\ 0 & 0 & 0 & 0 \\ 0 & 0 & 0 & 0 \\ 1 & 0 & 0 & 1 \end{bmatrix} - \frac{\epsilon J}{2} \begin{bmatrix} 1 & 0 & 0 & 0 \\ 0 & 0 & e^{-h} & 0 \\ 0 & e^{h} & 0 & 0 \\ 0 & 0 & 0 & 1 \end{bmatrix} \tag{4.46}$$

and so

$$\frac{\partial}{\partial h}\mathbb{T}_1 = -\frac{\epsilon J}{2}\begin{bmatrix} 0 & 0 & 0 & 0 \\ 0 & 0 & -e^{-h} & 0 \\ 0 & e^{h} & 0 & 0 \\ 0 & 0 & 0 & 0 \end{bmatrix}. \tag{4.47}$$

Given these expressions for $\mathbb{T}_1$ and $\frac{\partial}{\partial h}\mathbb{T}_1$written for space-like multiplication, one can easily verify that the choice

$$\mathbb{M} = \begin{bmatrix} 0 & 0 & 0 & 0 \\ 0 & -1 & 0 & 0 \\ 0 & 0 & 1 & 0 \\ 0 & 0 & 0 & 0 \end{bmatrix} \tag{4.48}$$

satisfies eq. (4.39). This $\mathbb{M}$ is in fact diagonal, and so it is not necessary to integrate over any extra spins. All that remains are the factors M determined by the two remaining spins. M will be non-zero only when $\mathbb{T}$ is a transition, and in fact, the resulting contribution is exactly that given by eq. (4.37).

The integral to calculate the particle number density thus becomes

$$\langle N\rangle = \frac{1}{LZ}\int [D\psi]\left(\sum_{t,\mu,x} M_{t,\mu,x}\right)\left(\prod_{t',\mu',x'} |T_{t',\mu',x'}|\right). \tag{4.49}$$

When the dust settles, the integral simply measures the difference between the number of instances of the two kinds of transitions on the lattice.

Interpreting M

Physical configurations on the $2+1$ dimensional lattice can be interpreted in terms of world lines for the spins, because the Hamiltonian commutes with the magnetization along the quantization axis:

$$\left[\mathbb{H}, \sum_z \mathbb{S}^3_z\right] = \left[J\sum_{x,\mu}\vec{\mathbb{S}}_x \cdot \left[\left(e^{-\delta_{\mu,1}ah\mathbb{S}^3_{x+\mu}}\right)\vec{\mathbb{S}}_{x+\mu}\left(e^{\delta_{\mu,1}ah\mathbb{S}^3_{x+\mu}}\right)\right], \sum_z \mathbb{S}^3_z\right] \tag{4.50}$$

$$= J\sum_{x,\mu,z}\left[\mathbb{S}^j_x\left[\left(e^{-\delta_{\mu,1}ah\mathbb{S}^3_{x+\mu}}\right)\mathbb{S}^j_{x+\mu}\left(e^{\delta_{\mu,1}ah\mathbb{S}^3_{x+\mu}}\right)\right], \mathbb{S}^3_z\right] \tag{4.51}$$

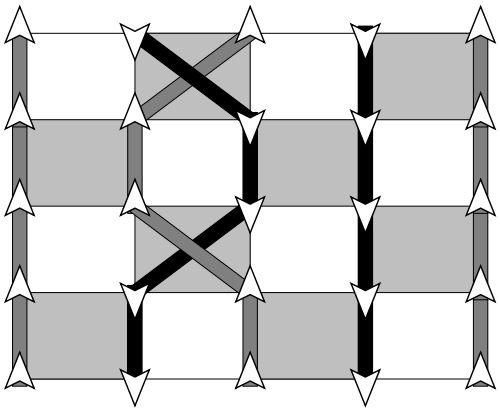

Figure 4-5: *The world lines of of up and down spins on a* $(1+1)D$ *lattice, in grey (▭) and black (▬) respectively. In this configuration, no world lines wind around the spatial direction.*

$$= J \sum_{x,\mu,z} \left[\begin{array}{l} [\mathbb{S}^j_x, \mathbb{S}^3_z] \left(e^{-\delta_{\mu,1} a h \mathbb{S}^3_{x+\mu}} \right) \mathbb{S}^j_{x+\mu} \left(e^{\delta_{\mu,1} a h \mathbb{S}^3_{x+\mu}} \right) \\ + \mathbb{S}^k_x \left(e^{-\delta_{\mu,1} a h \mathbb{S}^3_{x+\mu}} \right) [\mathbb{S}^k_{x+\mu}, \mathbb{S}^3_z] \left(e^{\delta_{\mu,1} a h \mathbb{S}^3_{x+\mu}} \right) \end{array} \right] \tag{4.52}$$

$$= J \sum_{x,\mu} \left[\begin{array}{l} i\epsilon^{j3l} \mathbb{S}^l_x \left(e^{-\delta_{\mu,1} a h \mathbb{S}^3_{x+\mu}} \right) \mathbb{S}^j_{x+\mu} \left(e^{\delta_{\mu,1} a h \mathbb{S}^3_{x+\mu}} \right) \\ + \mathbb{S}^k_x \left(e^{-\delta_{\mu,1} a h \mathbb{S}^3_{x+\mu}} \right) i\epsilon^{k3m} \mathbb{S}^m_{x+\mu} \left(e^{\delta_{\mu,1} a h \mathbb{S}^3_{x+\mu}} \right) \end{array} \right] \tag{4.53}$$

$$= J \sum_{x,\mu} \left[\mathbb{S}^l_x \left(e^{-\delta_{\mu,1} a h \mathbb{S}^3_{x+\mu}} \right) \mathbb{S}^j_{x+\mu} \left(e^{\delta_{\mu,1} a h \mathbb{S}^3_{x+\mu}} \right) \right] \left(i\epsilon^{j3l} + i\epsilon^{l3j} \right) \tag{4.54}$$

$$= 0 \tag{4.55}$$

Every plaquette on the lattice is either a continuation or a transition. On a continuation, the spins are understood to stay put spatially during that time slice. On a transition, the two spins at the bottom of the plaquette swap places on their way to the top. A typical spin configuration along with the world lines for a (1+1)D lattice is depicted in fig. 4-5. On one kind of transition, in their progress toward the top of the lattice, up spins hop right while down spins hop left. On the other kind of transition the opposite happens. Thus the difference between the numbers of the two kinds of transitions in the 1st direction is the winding of the up spins minus the winding of the down spins around the 1st direction.

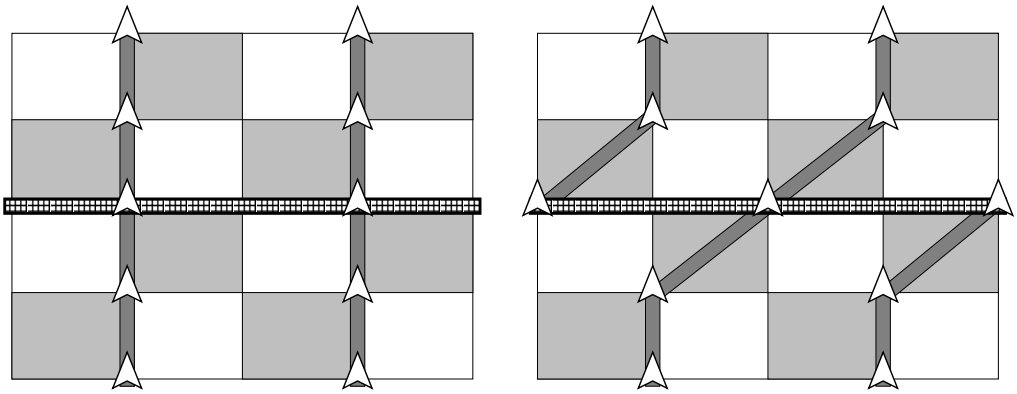

Figure 4-6: *A cluster changing the winding of the world lines. The world lines of up spins are shown in grey (▬). A cluster is shown in cross-hatching (▦). Down spins and their world lines are not shown. Flipping the cluster, which winds, changes the winding of the world lines.*

With this understanding of the particle number, one can better to understand the Metropolis weight for flipping the clusters. A cluster which itself winds is a cluster which when flipped will change the winding of the world lines, and hence the particle number. It is possible to simplify measuring the particle number, because the winding of the world lines can be measured by considering any one vertical plane through which the world lines must pass. The winding can be calculated by counting transitions in one spatial slice alone.

4.3.4 The Failure of this Method

This algorithm proves to be inefficient. The reasons for its failure are subtle, but the result is drastic. Although the Metropolis step is properly biased toward one orientation of each cluster which winds, the cluster rules are not biased to create such clusters. As a result, this algorithm does not effectively update the winding number. It is ergodic, so eventually it will explore different winding sectors. The construction of clusters which wind around the lattice is a rare event, however, and so the Metropolis step only very rarely gets a chance to impose its bias. In this formulation, the chemical potential has been somewhat crudely grafted onto the cluster algorithm. The result

is that the cluster growth is only indirectly and occasionally affected by the chemical potential and so the method is ineffective.

4.4 Quantize Transverse to the Chemical Potential

In contrast to the choice above, one can instead choose the quantization axis to be transverse to the chemical potential. This choice will lead to a sign problem, and so the inefficiency described above will not immediately vanish. By attacking this sign problem head on instead of avoiding it, however, one may fix the inefficiency.

4.4.1 The Basic Construction

Choosing $\vec{h}\cdot\vec{\sigma}$ to be $h\sigma_1$, the exponential in eq. (4.21) is this time[5]

$$\mathbb{I}\otimes\left(c_\mu\mathbb{I}+s_\mu\begin{bmatrix}0&1\\1&0\end{bmatrix}\right)=\mathbb{I}\otimes\begin{bmatrix}c_\mu&s_\mu\\s_\mu&c_\mu\end{bmatrix}. \tag{4.56}$$

For $\mu\neq 1$, T_μ will of course reduce to the $h=0$ case. Considering the $\mu=1$ case and suppressing the unnecessary index, now eq. (4.23) becomes

$$\begin{bmatrix}1&0\\0&0\end{bmatrix}\otimes\begin{bmatrix}-s^2&sc\\-sc&c^2\end{bmatrix}-\begin{bmatrix}0&1\\0&0\end{bmatrix}\otimes\begin{bmatrix}sc&-s^2\\c^2&-sc\end{bmatrix}-\begin{bmatrix}0&0\\1&0\end{bmatrix}\otimes\begin{bmatrix}-sc&c^2\\-s^2&sc\end{bmatrix}+\begin{bmatrix}0&0\\0&1\end{bmatrix}\otimes\begin{bmatrix}c^2&-sc\\sc&-s^2\end{bmatrix}$$
$$=\begin{bmatrix}-s^2&sc&-sc&s^2\\-sc&c^2&-c^2&sc\\sc&-c^2&c^2&-sc\\s^2&-sc&sc&-s^2\end{bmatrix}. \tag{4.57}$$

Discarding a multiplicative constant and expanding to first order in ϵ as before, for this choice of quantization axis,

$$\mathbb{T}_1\approx\begin{bmatrix}1-c^2\frac{\epsilon J}{2}&sc\frac{\epsilon J}{2}&-sc\frac{\epsilon J}{2}&s^2\frac{\epsilon J}{2}\\-sc\frac{\epsilon J}{2}&1+s^2\frac{\epsilon J}{2}&-c^2\frac{\epsilon J}{2}&sc\frac{\epsilon J}{2}\\sc\frac{\epsilon J}{2}&-c^2\frac{\epsilon J}{2}&1+s^2\frac{\epsilon J}{2}&-sc\frac{\epsilon J}{2}\\s^2\frac{\epsilon J}{2}&-sc\frac{\epsilon J}{2}&sc\frac{\epsilon J}{2}&1-c^2\frac{\epsilon J}{2}\end{bmatrix}. \tag{4.58}$$

[5]Again, h is taken to be positive w.l.o.g.

4.4.2 Breakups

Unlike the previous case, the transfer matrix has much more structure when $h \neq 0$ than when $h = 0$. Not only does it have some more negative entries, but it has none of the zeroes present in eq. (4.6). Moreover, there are lattice configurations for which the signs in this new transfer matrix do not cancel out – there is a sign problem.

The decomposition in terms of breakups used for the case of non-zero chemical potential will not be sufficient for this transfer matrix. Instead, it is necessary to go back to the transfer matrix and find a new set of breakups. To ensure that the reference configuration still be valid, all the bonds used in these new breakups should still be satisfied on the same staggered lattice which was the reference configuration with no h. The expansion of the new transfer matrix analogous to eq. (4.7) is:

$$\begin{aligned}\mathbb{T}_1 = &\left(1 - c^2\frac{\epsilon J}{2}\right)\begin{bmatrix}1&0&0&0\\0&1&0&0\\0&0&1&0\\0&0&0&1\end{bmatrix} + c\,(c-2s)\,\frac{\epsilon J}{2}\begin{bmatrix}0&0&0&0\\0&1&-1&0\\0&-1&1&0\\0&0&0&0\end{bmatrix}\\ &+ s^2\frac{\epsilon J}{2}\begin{bmatrix}0&0&0&1\\0&1&0&0\\0&0&1&0\\1&0&0&0\end{bmatrix} + sc\frac{\epsilon J}{2}\begin{bmatrix}0&0&0&0\\-1&1&-1&1\\1&-1&1&-1\\0&0&0&0\end{bmatrix} + sc\frac{\epsilon J}{2}\begin{bmatrix}0&1&-1&0\\0&1&-1&0\\0&-1&1&0\\0&-1&1&0\end{bmatrix}. \quad (4.59)\end{aligned}$$

The first two of these matrices appeared in the $h = 0$ case. The other three correspond to three new breakups depicted in table 4.4. The decomposition is summarized in table 4.5. The most notable feature of this new set of breakups is the appearance of unbonded sites. Each of the last two matrices above corresponds to a breakup with only a single bond. Thus the clusters in the new algorithm will not necessarily be closed loops – they may also be open chains. Note that unbonded sites come in pairs, as if some horizontal bonds had broken. Note also that horizontal bonds carry a sign, and so also does one piece of each unbonded pair. The remaining breakup corresponds to a pair of crossed bonds. Thus the shapes of clusters are much more complicated in this case than they were previously, as depicted in fig. 4-7.

Matrix	Diagram	Allowed configurations
$\begin{bmatrix} 0 & 0 & 0 & 1 \\ 0 & 1 & 0 & 0 \\ 0 & 0 & 1 & 0 \\ 1 & 0 & 0 & 0 \end{bmatrix}$		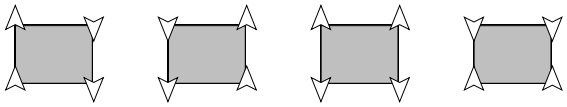
$\begin{bmatrix} 0 & 1 & -1 & 0 \\ 0 & 1 & -1 & 0 \\ 0 & -1 & 1 & 0 \\ 0 & -1 & 1 & 0 \end{bmatrix}$		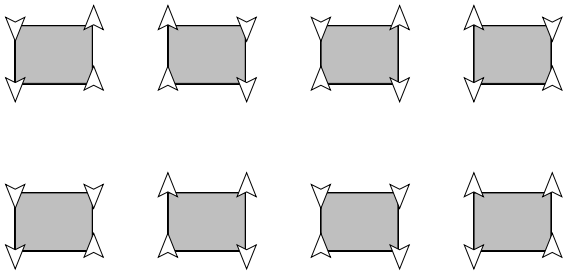
$\begin{bmatrix} 0 & 0 & 0 & 0 \\ -1 & 1 & -1 & 1 \\ 1 & -1 & 1 & -1 \\ 0 & 0 & 0 & 0 \end{bmatrix}$		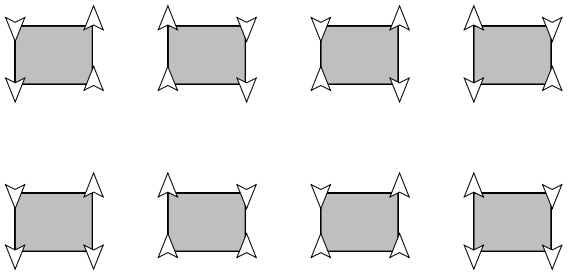

Table 4.4: *Three new breakups for* (1+1+1)D $O(3)$ *introduced by quantizing transverse to the chemical potential, and the spin configurations which satisfy them. As before, bonds are cross-hatched (▬) to indicate that the sign changes when they are flipped.*

Typical Spins	Total Weight	 $1-c^2\frac{\epsilon J}{2}$	 $c(c-2s)\frac{\epsilon J}{2}$	 $s^2\frac{\epsilon J}{2}$	 $sc\frac{\epsilon J}{2}$	 $sc\frac{\epsilon J}{2}$
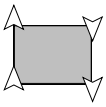	$1-s^2\frac{\epsilon J}{2}$	+	+	+	+	+
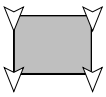	$1-c^2\frac{\epsilon J}{2}$	+				
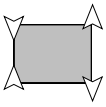	$-c^2\frac{\epsilon J}{2}$		−		−	−
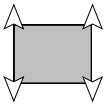	$s^2\frac{\epsilon J}{2}$			+		
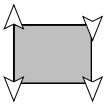	$sc\frac{\epsilon J}{2}$					+
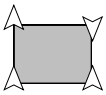	$-sc\frac{\epsilon J}{2}$					−
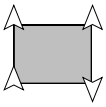	$sc\frac{\epsilon J}{2}$				+	
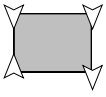	$-sc\frac{\epsilon J}{2}$				−	

Table 4.5: *The assignment of weights to the breakups when the quantization axis is transverse to the chemical potential. The structure is the same as in table 4.2.*

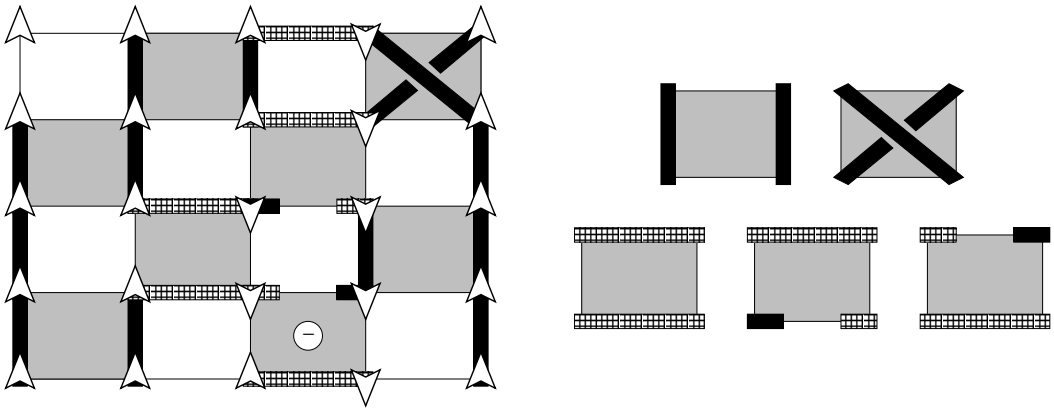

Figure 4-7: *A typical joint configuration of spins and clusters in a* $(1{+}1)D$ *Heisenberg antiferromagnet when the quantization axis is transverse to* $\vec{h}$*. The breakups used to build the cluster configuration are shown on the right. There are two open chains and one closed loop in this example. Only the longer chain is oriented against the reference configuration. The single minus sign marks the one plaquette on this lattice which has a spin configuration for which the sign is negative.*

4.4.3 Handling the Signs

In the $h = 0$ case, although there were signs associated with horizontal segments, clusters always had an even number of horizontal segments. *Because they had to be closed loops*, the signs always canceled. Now clusters can break open, and there is no such guarantee.

The sign$[\psi]$ does factor as required in eq. (2.31) because the global sign – a product over signs from plaquettes – has been written as a product over signs from bonds. By decomposing each plaquette sign into a product of signs from each bond, the sign has been split up into factors which can be grouped together by cluster. In the reference configuration, the sign is still positive, but now if a cluster has an odd number of segments with signs – those shown with cross-hatching (▭) – flipping that cluster will change the global sign. Such a cluster is called a *meron*.

Note that closed loop clusters are still never merons. Moreover, the only cluster segments with signs are either horizontal bonds or half of broken horizontal bonds. By imagining repairing the broken bonds, one should be able to see that the total

number of segments carrying signs must be even. Thus, if there are any merons, they must come in pairs.

Consider the (1+1)D example given in fig. 4-7, which has two merons. The short chain has one segment with a minus sign, and the long chain has three. The loop, being closed, must have an even number of horizontal segments and so is not a meron. Since exactly one of the two merons (the long chain) is oriented against the reference configuration, the configuration's global sign would be negative. One can check this by multiplying together the sign for each active plaquette. As indicated in the diagram, only one plaquette carries a minus sign, and so this calculation yields the same answer as predicted by the merons.

Having first determined that there are non-trivial signs, and then having constructed a cluster system with merons, one can now put into practice the general method described in section 2.2.4 and hence solve the sign problem. An improved estimator for the sign as in eq. (2.30) is simple to construct once merons have been identified.

The construction proceeds in precise analogy with eqs. (4.8)-(4.15), where in this case $n_b = 5$ and $\mathcal{O}[\psi] \equiv \text{sign}[\psi]$. As described in section 2.2.4, if there are any merons then in averaging over all cluster orientations one half will have the opposite sign from the other, and the average will be zero. If there are no merons the sign will never change; since the sign is known to be positive in the reference configuration, the average of the sign in a case with no merons must be one.

Thus an importance sampling ensemble can be constructed with a proper sense of importance. Configurations which have merons, regardless of the weight determined by the magnitude of the transfer matrix elements, are not important – they contribute zero to the average of the sign. Hence the ensemble should be reweighted to reflect a bias against merons.

Thus the solution to this sign problem proceeds in two steps. The meron concept is used to construct an improved estimator for the sign, which for every cluster configuration produces either 0 or 1. Although there are no more negative contributions and hence no more cancellation, this step alone does not solve the sign problem. Since

the result of the average is known to be exponentially small in the volume, there must be very few 1s amid a sea of 0s. By subsequently reweighting the ensemble, biasing it toward configurations which are truly significant, the sea of 0s can be avoided, and the algorithm thus made to be efficient.

4.4.4 Measuring The Particle Number Density

Because there is a sign problem to be solved, observables must now be estimated using eq. (2.35). The method of direct element-by-element differentiation used first for the previous choice of quantization axis is very messy in this case. Every element of $\mathbb{T}$ has some h dependence, and so the result of the differentiation is very complicated. The second method – finding an operator to insert – is easier.

Returning to the new transfer matrix and applying the rearrangement described by eq. (4.43), the transfer matrix $\mathbb{T}_1$ from eq. (4.58) changes as follows:

$$\mathbb{T}_1 = \begin{bmatrix} 1 - c^2\frac{\epsilon J}{2} & sc\frac{\epsilon J}{2} & -sc\frac{\epsilon J}{2} & s^2\frac{\epsilon J}{2} \\ -sc\frac{\epsilon J}{2} & 1 + s^2\frac{\epsilon J}{2} & -c^2\frac{\epsilon J}{2} & sc\frac{\epsilon J}{2} \\ sc\frac{\epsilon J}{2} & -c^2\frac{\epsilon J}{2} & 1 + s^2\frac{\epsilon J}{2} & -sc\frac{\epsilon J}{2} \\ s^2\frac{\epsilon J}{2} & -sc\frac{\epsilon J}{2} & sc\frac{\epsilon J}{2} & 1 - c^2\frac{\epsilon J}{2} \end{bmatrix} \tag{4.60}$$

$$= \begin{bmatrix} 1 & 0 & 0 & 0 \\ 0 & 1 & 0 & 0 \\ 0 & 0 & 1 & 0 \\ 0 & 0 & 0 & 1 \end{bmatrix} + \frac{\epsilon J}{2} \begin{bmatrix} -c^2 & sc & -sc & s^2 \\ -sc & s^2 & -c^2 & sc \\ sc & -c^2 & s^2 & -sc \\ s^2 & -sc & sc & -c^2 \end{bmatrix} \tag{4.61}$$

$$\longrightarrow \begin{bmatrix} 1 & 0 & 0 & 1 \\ 0 & 0 & 0 & 0 \\ 0 & 0 & 0 & 0 \\ 1 & 0 & 0 & 1 \end{bmatrix} + \frac{\epsilon J}{2} \begin{bmatrix} -c^2 & sc & -sc & s^2 \\ -sc & s^2 & -c^2 & sc \\ sc & -c^2 & s^2 & -sc \\ s^2 & -sc & sc & -c^2 \end{bmatrix} \tag{4.62}$$

and so

$$\frac{\partial}{\partial h}\mathbb{T}_1 = \frac{\epsilon J}{4} \begin{bmatrix} -2sc & s^2 + c^2 & -s^2 - c^2 & 2sc \\ -s^2 - c^2 & 2sc & -2sc & s^2 + c^2 \\ s^2 + c^2 & -2sc & 2sc & -s^2 - c^2 \\ 2sc & -s^2 - c^2 & s^2 + c^2 & -2sc \end{bmatrix} \tag{4.63}$$

$$= \frac{1}{2} \begin{bmatrix} 0 & 1 & -1 & 0 \\ 1 & 0 & 0 & -1 \\ -1 & 0 & 0 & 1 \\ 0 & -1 & 1 & 0 \end{bmatrix} \star \mathbb{T}. \tag{4.64}$$

Hence $\mathbb{M}$, the operator inserted to compute the particle number, can be taken to be

$$\mathbb{M} = \frac{1}{2} \begin{bmatrix} 0 & 1 & -1 & 0 \\ 1 & 0 & 0 & -1 \\ -1 & 0 & 0 & 1 \\ 0 & -1 & 1 & 0 \end{bmatrix} \tag{4.65}$$

This matrix is not diagonal, so its operation in the context of the path integral is more complicated than was that of the equivalent matrix with the other quantization axis. In order better to understand the action of $\mathbb{M}$, define

$$\mathbb{M}_l \equiv \frac{1}{2} \begin{bmatrix} 0 & 0 & 1 & 0 \\ 0 & 0 & 0 & 1 \\ 1 & 0 & 0 & 0 \\ 0 & 1 & 0 & 0 \end{bmatrix} \qquad \text{and} \qquad \mathbb{M}_u \equiv \frac{1}{2} \begin{bmatrix} 0 & 1 & 0 & 0 \\ 1 & 0 & 0 & 0 \\ 0 & 0 & 0 & 1 \\ 0 & 0 & 1 & 0 \end{bmatrix} \tag{4.66}$$

so that $\mathbb{M} = \mathbb{M}_u - \mathbb{M}_l$. This decomposition separates $\mathbb{M}$ into two parts each of which is block anti-diagonal. If not diagonal, these are at least deterministic in that if they act on a single state in the path integral the result will not be a superposition of states. Instead, the result will be another element of the basis in which the path integral is being calculated. In fact, the insertion of either of these operators flips a single spin in its passage sideways. $\mathbb{M}_l$ flips the lower one and $\mathbb{M}_u$ flips the upper one, as shown in fig. 4-8.

Because these matrices change spins, the physical configurations generated for evaluating the expectation value of the sign – the denominator in eq. (2.23) – are not directly usable for evaluating the integral in the numerator. For any insertion of an $\mathbb{M}$, those physical configurations lack the extra spins inserted between the transfer matrix and the $\mathbb{M}$.

However, although the spin configuration is not usable, the *cluster* configuration is usable[12]. For the deterministic $\mathbb{M}_u$ and $\mathbb{M}_l$, a given cluster configuration – formerly meaning a constraint on the lattice without any $\mathbb{M}$ – can be reinterpreted to mean also a different constraint on the lattice with one inserted $\mathbb{M}$.

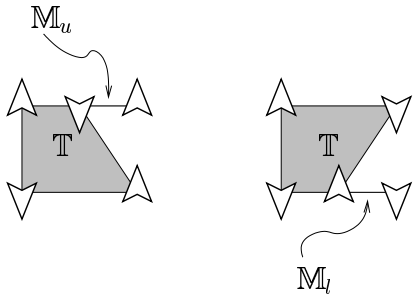

Figure 4-8: *The effect of inserting the non-diagonal* $\mathbb{M}_u$ *and* $\mathbb{M}_l$*. These two matrices respectively flip the upper and lower spin on a plaquette as it proceeds sideways after the action of* $\mathbb{T}$*.*

The insertion of $\mathbb{M}_u$ or $\mathbb{M}_l$ at one plaquette on the lattice has the effect of flipping one spin as it proceeds sideways. As a cluster crosses the site where an $\mathbb{M}$ is affecting a spin, the orientation of the cluster changes. If it is aligned with the reference configuration on one side of the insertion, then it is aligned against it on the other. An example is shown in fig. 4-9.

Because only one $\mathbb{M}$ is inserted into the lattice at a time, there will be exactly one such extra flip imposed on the lattice at a time. Closed clusters will therefore produce no contribution, as the two parts of the cluster forced at the insertion to be differently oriented will be connected elsewhere. When an open cluster passes through the insertion the $\mathbb{M}$ will produce a contribution of $\frac{1}{2}$ or $-\frac{1}{2}$, depending on whether the insertion is at an upper or a lower spin. This contribution will, in turn, be multiplied by the global sign.

Since merons come in pairs, the value of the improved estimator must be zero if there are any merons. Although the insertion of an $\mathbb{M}$ may affect one meron, there will always be another to flip and cancel out any contribution. Suppose, however, that an insertion should happen to land in an open chain which has an even number of signed segments. Suppose further that it should split the cluster into two halves each of which has an *odd* number of signed segments. In such a case, no matter how the cluster is flipped, half of it will be against the reference configuration and that half will carry a sign. Hence there will be an extra sign.

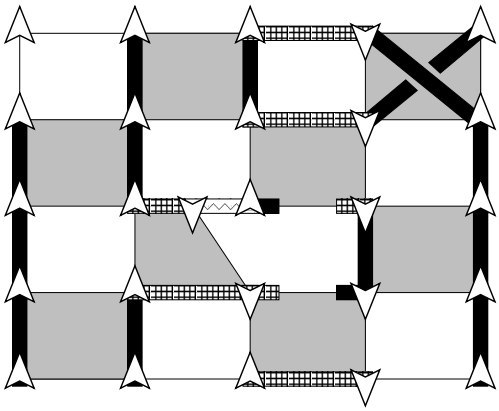

Figure 4-9: *Computing an observable with the non-diagonal* $\mathbb{M}_u$*. The insertion of* $\mathbb{M}_u$ *has changed the interpretation of the longer open chain. The chain still has just two orientations, but where it crosses the insertion (▭), the orientation changes. Compare this to fig. 4-7, which has the same cluster configuration with no insertion.*

Interpreting $\mathbb{M}$

As with the previous choice of quantization axis, further geometrical interpretation of the insertion of $\mathbb{M}$ can provide insight into the nature of the improved estimator. Whenever cluster segments step horizontally in the direction of the chemical potential, the contributions accumulate. Whenever cluster segments step vertically, the contributions cancel out. The contributions from $\mathbb{M}$ add up to measure a winding number – this time of the loops which would result from reconnecting the open clusters. An example in (1+1)D is given in fig. 4-10. The (2+1)D case is of course more complicated, but the result is the same.

When the spins were quantized parallel to $\vec{h}$, the cluster algorithm is inefficient because it is necessary for the clusters themselves to wind around the lattice in order to change a winding number. At any finite correlation length, that is a rare event on a large enough lattice, and so the update becomes less and less effective as the lattice gets bigger. Now, with the spins quantized transverse to $\vec{h}$, updating the relevant winding number no longer requires a cluster which itself winds. Instead, many small clusters may conspire to wind as a whole. Thus the original inefficiency is not present.

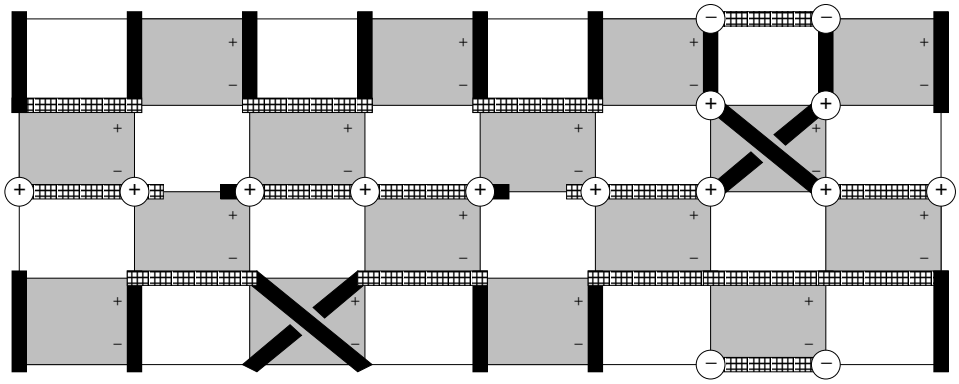

Figure 4-10: *Calculating the particle number when the quantization axis is transverse to the chemical potential, in* (1+1)*D. The signs on the grey transfer matrices indicate the sign contributed by* $\mathbb{M}_l$ *or* $\mathbb{M}_u$*. The signs in white circle indicate the final contributions from the improved estimator. On the closed cluster, there are no contributions. On the open clusters, the sign contributed by* $\mathbb{M}$ *is multiplied by a sign from how the cluster is split: if the site splits the cluster into pieces with an odd number of signed segments, there is an extra sign. The contributions add up to measure the winding number of the reconnected open clusters.*

4.4.5 The Sign Problem is Solved

Quantizing the spins transverse to the chemical potential results in a sign problem. By expressing the path integral in terms of a cluster algorithm, it is possible to bring that sign problem under control. The structure of the cluster algorithm – breaking down the transfer matrix in terms of breakups and bonds – provides a rich structure in which to seek a solution. By expressing the global sign in terms of factors attributable to each cluster and its respective orientation, an improved estimator for the sign can be constructed. With that powerful tool in hand, the importance sampling ensemble can be reweighted to use a more accurate notion of importance, and so an ensemble useful for making measurements can be generated practically.

Chapter 5

Numerical Results for (1+1+1)D $O(3)$

The meron algorithm including the improved estimator for the particle number density described in section 4.4 was applied on successively larger lattices, and so numerical estimates were generated for $\langle N \rangle$ as a function of h.

In this chapter, the physical extent of the spatial dimension of the 1+1 dimensional $O(3)$ theory shall be called L, the inverse temperature of the 1+1 dimensional system shall be called L', and the extent of the third dimension – the inverse temperature of the Heisenberg magnet – shall be called β. The factor ϵ determining the quality of the Trotter approximation is thus $\frac{\beta}{n}$ where n is the number of time slices introduced in the path integral.

For all the calculations in this chapter, the coupling constant of the magnet J – redundant except for its sign – was taken to be 1. The mass gap m is determined by β as described in eq. (3.12). The actual value of m as thus determined was taken from a numerical study of the correlation length $\xi = \frac{1}{m}$ in the Heisenberg antiferromagnet [5], as was the value of the magnon velocity $c = 0.1657(2)$.

Except where stated otherwise, the value $\beta = 2.5$ was used. This corresponds to $\xi = 6.23(1)$ and $m = 0.160(5)$. This is a relatively modest choice for β. Dimensional reduction occurs in the limit in which $\xi \gg \beta c$, but with this choice $\beta c = 4.143$, which is only somewhat smaller than ξ.

5.1 The Severity of the Sign Problem

In order better to understand the severity of the sign problem, the algorithm was run without any reweighting, allowing merons to develop unhindered. The resulting distributions of meron counts, plotted in fig. 5-1, make clearer the nature of the problem. At very small lattice sizes, only a few merons will fit on the lattice, but, once the lattice reaches reasonable sizes, the vast majority of the configuration space is occupied by the higher meron count sectors. All configurations which make non-zero contributions to the expectation value of the sign lie in the zero meron sector, which comprises only a tiny fraction of the configuration space at a far end of one tail of the distribution of meron counts.

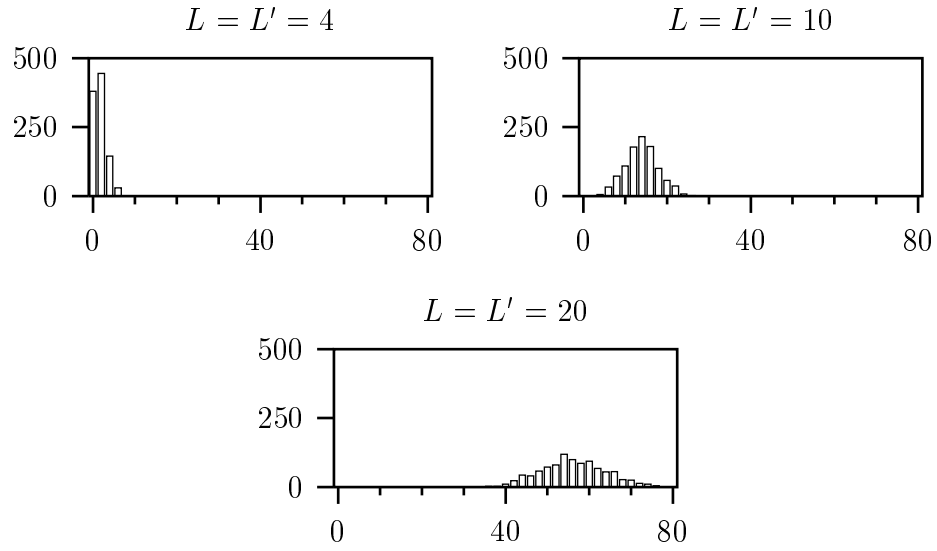

Figure 5-1: *Meron distribution as a function of system size. The algorithm was run for* 1000 *sweeps after* 100 *sweeps for thermalization at* $h = 0.15$*, for three* (L, L') *pairs.*

To see the effect of the reweighting, the algorithm was run at progressively larger values of the reweighting. The effect of the reweight is shown in fig. 5-2. For a reweight factor of r, the weight in the distribution of a configuration with n_m merons was thus artificially suppressed by a factor of r^{n_m}. Any contribution from a configuration with merons would in principle need to be inflated by a corresponding factor. However,

for both the quantities measured, all contributions in the non-zero meron sectors are identically zero. Thus the reweight serves *only* to amplify the measured signal relative to the statistical noise in the ensemble.

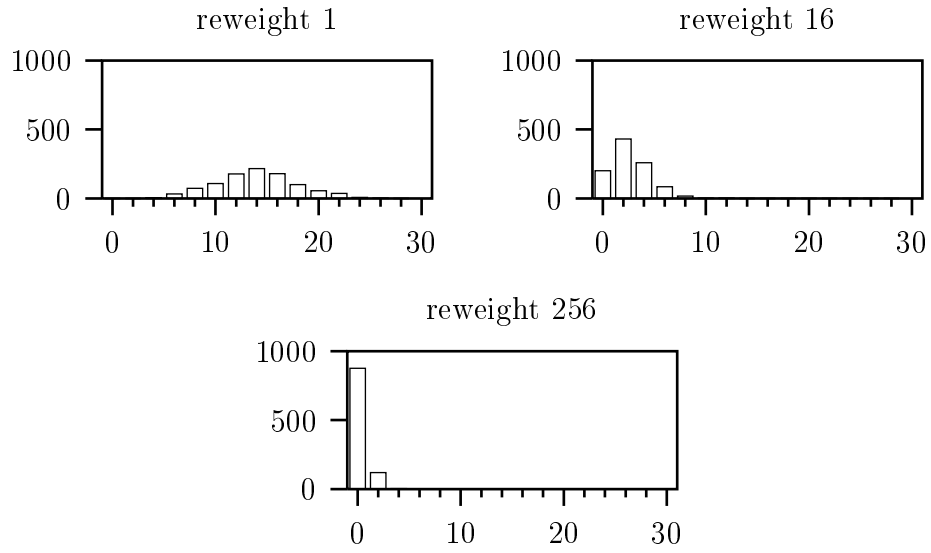

Figure 5-2: *The effect of reweighting on meron distribution in* (1+1+1)D $O(3)$ *when the quantization axis is transverse to the chemical potential. The algorithm was run for* 1000 *sweeps after* 100 *sweeps for thermalization, at* $L = 10$, $L' = 10$ *and* $h = 0.15$, *for three reweights,* 1, 16, *and* 256.

5.2 Particle Number Density

The algorithm was finally run with full reweighting at several lattice sizes, and the particle number density was measured as a function of chemical potential. A small Markov step was used, in which a single plaquette was updated. A large composite Markov step or *sweep* was made by sequentially choosing N_p plaquettes at random and updating them, where N_p is the number of plaquettes on the lattice. The value of the improved estimators for the particle number and sign were measured after each sweep.

For each value of h on each lattice size, several runs were made in parallel. Each run began with $N_{\rm therm}$ sweeps of the lattice without measurements in order to let

the lattice thermalize. After this thermalization, N_{sweep} sweeps were made in total across all parallel runs. These N_{sweep} measurements were grouped into blocks of N_{est} and an estimate was calculated from each block according to eq. (2.24). These $\frac{N_{\text{sweep}}}{N_{\text{est}}}$ estimates were then averaged to yield a final data point, and their deviation calculated to yield an error estimate. The block size of N_{est} was chosen to insure that any autocorrelation would not cause the errors to be underestimated.

5.2.1 $L = L' = 20$

For the $L = L' = 20$ lattice, $\beta = 2.5$, and $n = 50$ were used, resulting in $\epsilon = 0.05$. The data were generated using $N_{\text{therm}} = 500$, with $N_{\text{sweep}} = 8000$ grouped by blocks of $N_{\text{est}} = 1600$. The data calculated are listed in table 5.1, and plotted in fig. 5-3. The meron algorithm successfully solves the sign problem; statistical errors are well under control.

The validity of the Trotter expansion was verified by comparing – for a single value of h – the result for $\epsilon = 0.05$ with a second calculation at $\epsilon' \equiv \frac{\epsilon}{2}$. The value of h chosen was 0.13, and at the stated $\epsilon' = 0.025$ the value calculated was $\langle N \rangle = 0.018 \pm 0.0005$, in which is indeed compatible with the value from the table of $\langle N \rangle = 0.019 \pm 0.0010$.

In order to check that the spatial discretization was sufficient, a data point was generated at a longer correlation length on a correspondingly larger lattice. Referring again to previously calculated values of the correlation length [5], β was chosen to be 3.0 so as roughly to double ξ: at this value of $\beta = 3.0$ the correlation length is $\xi = 11.60$. At the same time, the number of sites in each spatial direction on the lattice was doubled, yielding $L = L' = 40$. The same Trotter discretization of $\epsilon = 0.05$ was used. A single data point was generated for at $h = 0.055$, yielding $\langle N \rangle = 0.0065 \pm 0.00045$. This datum may be reinterpreted as a measurement for $L = L' = 20$ with the lattice spacing a halved. In this interpretation, h would be $2 \times 0.005 = 0.11$, the correlation length would be $\frac{1}{2} \times 11.60 = 5.8$, and the mass gap would be $m = 0.172(4)$. Correspondingly $\langle N \rangle$ would be 0.013 ± 0.00090. Thus the lattice discretization has effectively been refined by a factor of two. The corresponding estimate from the fermion gas model is $\langle N \rangle = 0.012$.

h	$L = L' = 20$		$L = L' = 30$	
	$\langle N \rangle$	$\Delta\langle N \rangle$	$\langle N \rangle$	$\Delta\langle N \rangle$
0.01	0.00093	0.000068	0.00014	0.000047
0.03	0.0024	0.00022	0.00079	0.000066
0.05	0.0040	0.00023	0.0014	0.00012
0.07	0.0066	0.00035	0.0027	0.00014
0.09	0.0089	0.00044	0.0048	0.00032
0.11	0.014	0.0012	0.0082	0.00053
0.13	0.019	0.0010	0.0135	0.00048
0.15	0.028	0.0019	0.0236	0.00097
0.17	0.037	0.0014	0.0316	0.00094
0.19	0.047	0.0021	0.049	0.0015
0.21	0.054	0.0042	0.060	0.0018
0.23	0.073	0.0054	0.073	0.0023
0.25	0.085	0.0050	0.085	0.0023
0.27	0.100	0.0024	0.107	0.0012
0.29	0.11	0.011	0.119	0.0022

Table 5.1: *Numerical results for the particle number density in* (1+1+1)D $O(3)$

5.2.2 $L = L' = 30$

For the $L = L' = 30$ lattice $\beta = 2.5$ and $n = 25$ was used, resulting in $\epsilon = 0.1$. The data were generated using $N_{\text{therm}} = 1000$, with $N_{\text{sweep}} = 8000$ grouped by blocks of $N_{\text{est}} = 1000$. The data calculated are listed in table 5.1, and plotted in fig. 5-3. Again, statistical errors are well under control. The validity of the Trotter expansion was again verified this time with a second calculation at $\epsilon' \equiv \frac{\epsilon}{2} = 0.05$. The value of h chosen was 0.07, and at $\epsilon' = 0.05$ the value calculated was $\langle N \rangle = 0.0027 \pm 0.00022$. Again, this is compatible with the value in the table calculated at the larger value of $\epsilon = 0.1$, $\langle N \rangle = 0.0027 \pm 0.00014$.

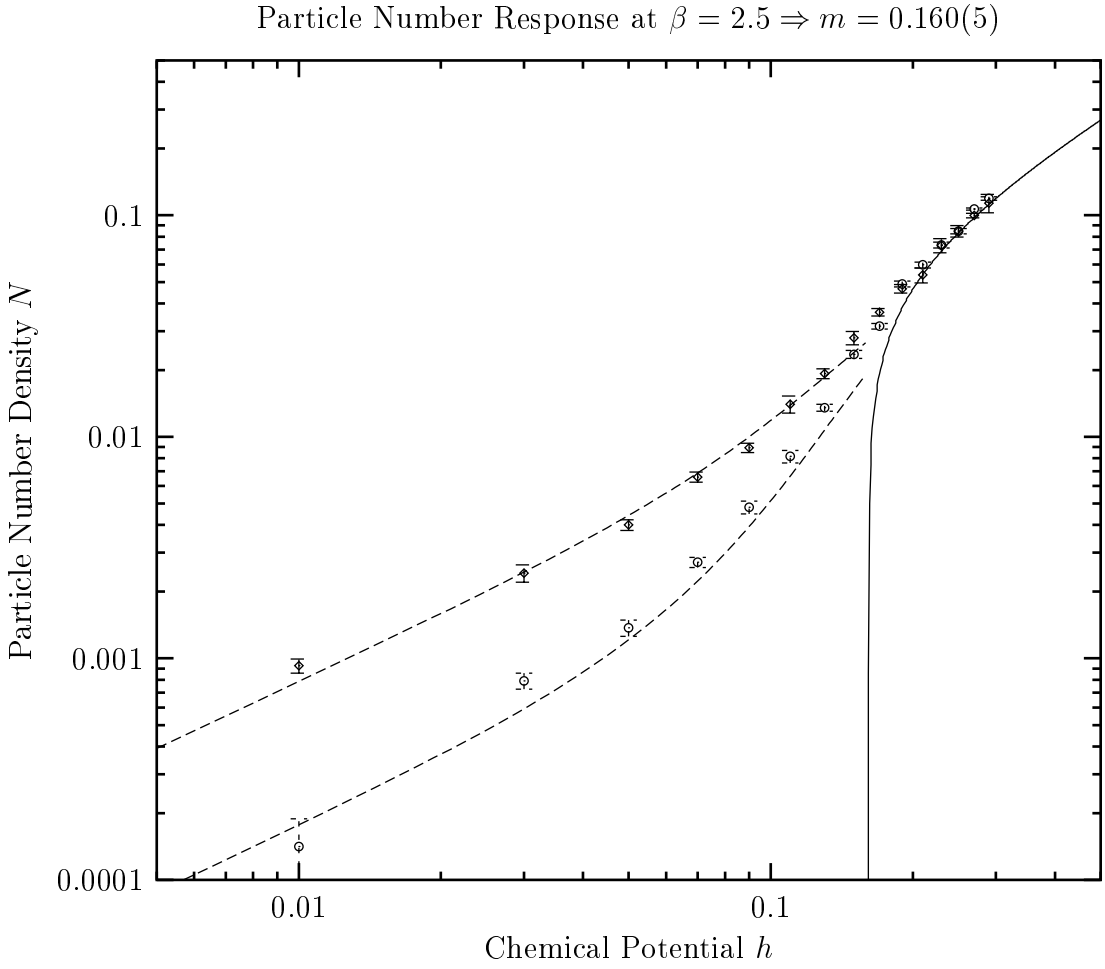

Figure 5-3: *Numerical results for the particle number density at* $L = L' = 20$ *and* $L = L' = 30$. *The solid line is the Bethe ansatz result for the* $L = L' = \infty$ *limit. The upper and lower dashed lines are the dilute fermion gas estimates from eq. (3.31) respectively for* $L = L' = 20$ *and* $L = L' = 30$. *Especially given that for this* β *the system is not very far into the dimensionally reduced limit, the agreement with the fermion and Bethe ansatz models is quite good.*

Chapter 6

Antiferromagnetic Spin Ladders in a Magnetic Field

The $2+1$ dimensional Heisenberg antiferromagnet has thus far been used because it is a D-Theory formulation of 1+1D $O(3)$ field theory, but it is an interesting system in its own right.

The introduction of the chemical potential in the previous chapters was, there, the cause of an inefficiency which could manifest itself as sign problem. However, the modification made to the antiferromagnet's Hamiltonian in order to add a chemical potential to the dimensionally reduced theory had no direct interpretation for the physical magnet. In fact, simply introducing a chemical potential directly to the 2+1 dimensional antiferromagnet causes a very similar inefficiency. Such a chemical potential is physically realized as an external magnetic field.

When one of the two spatial dimensions of a two dimensional magnet is very small, such a system is called a *spin ladder*. Such ladders in magnetic fields are yet another strongly coupled system which encounters a sign problem when a chemical potential is introduced. Thus this system is another good candidate for solving a sign problem using meron techniques [18].

6.1 The Physical System

A general antiferromagnetic Heisenberg spin ladder (with isotropic couplings) in a magnetic field $\vec{B}$ is described by the Hamiltonian operator

$$\mathbb{H} = \sum_{x=1}^{L} \sum_{y=1}^{L'} \left[J \sum_{\mu \in \{\hat{x}, \hat{y}\}} \vec{\mathbb{S}}_{(x,y)} \cdot \vec{\mathbb{S}}_{(x,y)+\mu} - \vec{B} \cdot \vec{\mathbb{S}}_{(x,y)} \right] \tag{6.1}$$

with $J > 0$, where $L' \ll L$.

Such spin ladders interpolate between one and two dimensional spin systems. Wider ladders approach being fully two dimensional systems. Narrower ladders are like one dimensional chains of spins – the spins on each rung of the ladder couple together to form a larger effective spin.

The full $2+1$ dimensional magnet – the case when both L and L' are large – has been discussed in chapter 3. Its low energy dynamics are described by the three dimensional effective action given in eq. (3.7):

$$S[\hat{e}] = \int_0^\beta dt \int d^2x \, \frac{\rho_s}{2} \left(\partial_\mu \hat{e} \cdot \partial_\mu \hat{e} + \frac{1}{c^2} \partial_t \hat{e} \cdot \partial_t \hat{e} \right) \tag{6.2}$$

For the other limit, the one dimensional case when $L' = 1$, Haldane conjectured [30] that a one dimensional length L chain of spin-S spins at temperature β is described by a similar continuum field theory, this time in 1+1 dimensions, with action

$$S[\hat{e}] = \int_0^\beta c dt \int_0^L dx \left[\frac{1}{2g^2} \left(\partial_x \hat{e} \cdot \partial_x \hat{e} + \frac{1}{c^2} \partial_t \hat{e} \cdot \partial_t \hat{e} \right) + \frac{i\theta}{4\pi} \hat{e} \cdot (\partial_x \hat{e} \times \partial_t \hat{e}) \right]. \tag{6.3}$$

Here the coupling constant g is given by $\frac{1}{g} = \frac{S}{2}$ for large S, and the vacuum angle θ is given by $2\pi S$. For half integer spin and hence $\theta = \pi$, this system has no mass gap. However, $\theta = 0$ when the spin is an integer. In that case, after scaling out c, this system is another version of the (1+1)D continuum theory described in chapter 3, and it has a mass gap $m \propto e^{-\frac{2\pi}{g}}$.

As reviewed in [26], Haldane's result has been extended to spin ladders: ladders consisting of an odd number of transversely coupled spin 1/2 chains are gapless, while

ladders consisting of an even number of chains have a gap [36, 49, 46]. If the number of chains is kept even, these intermediate systems are described by the action

$$S[\hat{e}] = \int_0^\beta dt \int_0^L dx \int_0^{L'} dy \; \frac{\rho_s}{2}[\partial_x \hat{e} \cdot \partial_x \hat{e} + \partial_y \hat{e} \cdot \partial_y \hat{e} + \frac{1}{c^2}\partial_t \hat{e} \cdot \partial_t \hat{e}]. \tag{6.4}$$

As L' – the width of the ladder – is increased (keeping the number of spins even), the effective spin S of a step on the ladder increases and the gap $m \propto e^{-\frac{2\pi}{g}} = e^{-\pi S}$ decreases exponentially. Thus the ladder behaves very much like a rotated version of the system considered in the previous chapters – the ladder can be made to undergo dimensional reduction. Previously, the extent of the third dimension was made small in the physical units of the correlation length by increasing β. Now, the extent of the second direction – the width of the ladder – can be made small by increasing L'.

Introducing an external magnetic field has an analogous effect to the introduction of the chemical potential to the 1+1 dimensional $O(3)$ field theory in section 3.2.1. The magnetic field is coupled to the magnetization – the conserved charge of the global $O(3)$ symmetry – hence it is a chemical potential. It is therefore introduced into the continuum action (6.4) as a constant, imaginary, time-like gauge field. Section 3.2.1 introduced a chemical potential to a (1+1)D theory, so there "time-like" meant the one of two directions – in that case the first. Here, the magnetic field $\vec{B}$ will be introduced to a $(2+1)$D system, and so "time-like" will mean the third direction. Thus the derivative $\partial_t \hat{e}$ will become $\partial_t \hat{e} + i\vec{B} \times \hat{e}$, and the continuum action will become

$$S[\hat{e}] = \int_0^\beta dt \int_0^L dx \int_0^{L'} dy \; \frac{\rho_s}{2} \left[\partial_x \hat{e} \cdot \partial_x \hat{e} + \partial_y \hat{e} \cdot \partial_y \hat{e} + \frac{1}{c^2}(\partial_t \hat{e} + i\vec{B} \times \hat{e}) \cdot (\partial_t \hat{e} + i\vec{B} \times \hat{e}) \right]. \tag{6.5}$$

As described above, for sufficiently large L' (meaning $L' \gg \frac{\rho_s}{c}$) this system will undergo dimensional reduction, and the correlation length will become large compared to L'. At that point, y may be integrated out of eq. (6.5). The result is an effective

action for a 1+1 dimensional $O(3)$ field theory:

$$S[\hat{e}] = \int_0^\beta dt \int_0^L dx \frac{\rho_s L'}{2} \left[\partial_x \hat{e} \cdot \partial_x \hat{e} + \frac{1}{c^2} (\partial_t \hat{e} + i\vec{B} \times \hat{e}) \cdot (\partial_t \hat{e} + i\vec{B} \times \hat{e}) \right]. \tag{6.6}$$

Comparing this action to eq. (3.17), one can see that the original (1+1)D theory with chemical potential will be recovered if $\frac{1}{g^2} = \frac{\rho_s L'}{2}$ and $\vec{h} = \frac{\vec{B}}{c}$. With this identification in mind, the exact results listed in section 3.2.3 can be used for comparison with numerical results for the dimensionally reduced limit of the spin ladder, just as they were for the previous algorithm.

6.2 Constructing a Cluster Algorithm

In the absence of a magnetic field, antiferromagnetic spin systems can be simulated with the loop cluster algorithm described in section 4.1. As in chapter 4, there is a choice of axis for quantizing the spins. Quantizing along the magnetic field changes the weights of clusters which wind; quantizing transverse to the field causes the cluster loops to break open. The details from which these properties arise, however, are different because the magnetic field acts in the same direction as the Hamiltonian. Thus the construction of cluster algorithms for the antiferromagnet in a magnetic field is another instructive example of the application of merons to solving sign problems.

6.2.1 Introducing the Field

As shown in eq. (6.1), the introduction of the magnetic field adds a term to the Hamiltonian. Because of this simple additive structure, the only change which needs to be made to the path integral is the introduction of an additional slice in the Trotter decomposition. The decomposition given in eq. (2.2) is modified to become

$$e^{-\epsilon \mathbb{H}} = e^{-\epsilon \sum_x \left[\sum_\mu \mathbb{H}_{x,\mu} + \mathbb{H}_x \right]} \approx \left[\prod_\mu \left(\prod_x e^{-\epsilon \mathbb{H}_{x,\mu}} \right) \right] \prod_x e^{-\epsilon \mathbb{H}_x}. \tag{6.7}$$

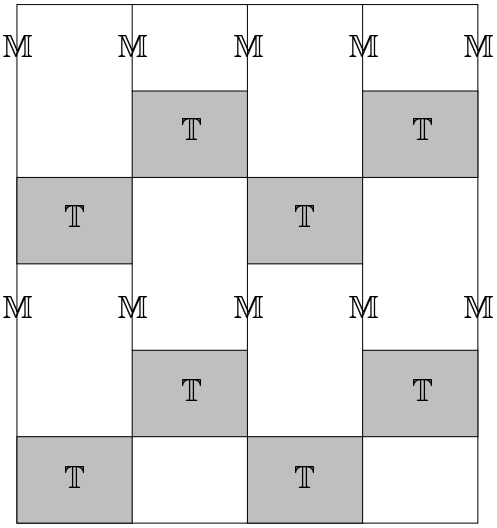

Figure 6-1: *A (1+1)D lattice with a extra slices inserted for the action of* $\vec{B}$*. The operators* $\mathbb{T}$ *act on plaquettes, but the operators* $\mathbb{M}$ *act just on time-like links.*

Here x represents all spatial coordinates. $\mathbb{H}$ has been decomposed into a bond interaction term $\mathbb{H}_{x,\mu}$ for the bond between x and $x+\mu$, and a local term $\mathbb{H}_x$. The result of adding the magnetic field is thus to add an extra slice to the lattice after each set of slices for a given value of t. The form of the partition function used for these simulations will thus be

$$Z = \int [D\psi] \prod_t \left[\left(\prod_{\mu,x} T_{t,\mu,x} \right) \prod_x M_{t,x} \right]. \tag{6.8}$$

Here M sits in the new time slice – i.e.

$$M_{t,x} = \langle \psi_{t+1,+\hat{x},x} | \mathbb{M}_{t,x} | \psi_{t,-\hat{y},x} \rangle. \tag{6.9}$$

The structure of this modified lattice is shown in fig. 6-1.

The transfer matrix $\mathbb{T}$ is not modified by the introduction of the field – it is still given by eq. (4.6), and it will still be decomposed into breakups according to eq. (4.5).

The operator $\mathbb{M}_{t,x}$ arises directly from the new $-\vec{B}\cdot\vec{\mathbb{S}}$ term:

$$\mathbb{M} = e^{\epsilon\vec{B}\cdot\vec{\mathbb{S}}}. \tag{6.10}$$

Quantizing Parallel to the Field

When the quantization axis is chosen to be parallel to the field, $\mathbb{M}$ is given by

$$\mathbb{M} = e^{\epsilon B\mathbb{S}_3} = e^{\frac{\epsilon B}{2}\sigma_3} = \begin{bmatrix} e^{\frac{\epsilon B}{2}} & 0 \\ 0 & e^{-\frac{\epsilon B}{2}} \end{bmatrix}. \tag{6.11}$$

Because this $\mathbb{M}$ is diagonal, it does not change the shapes of the clusters. There is only one breakup for the $\mathbb{M}$ links, and it bonds the bottom site to the top site. Instead the weights of the different orientations for clusters which wind around the time direction must change.

The magnetization induced by the magnetic field is proportional to the difference between the total number of up spins and down spins. The world line interpretation discussed in section 4.3.3 is again valid for this choice of quantization, because the Hamiltonian again commutes with the magnetization along the quantization axis:

$$\left[\mathbb{H}, \sum_z \mathbb{S}_z^3\right] = \left[\left(J\sum_{x,\mu}\vec{\mathbb{S}}_x\cdot\vec{\mathbb{S}}_{x+\mu} - B\sum_x \mathbb{S}_x^3\right), \sum_z \mathbb{S}_z^3\right] \tag{6.12}$$

$$= J\sum_{x,\mu,z}\left[\mathbb{S}_x^j\mathbb{S}_{x+\mu}^j, \mathbb{S}_z^3\right] - 0 \tag{6.13}$$

$$= J\sum_{x,\mu,z}\left[\left[\mathbb{S}_x^j, \mathbb{S}_z^3\right]\mathbb{S}_{x+\mu}^j + \mathbb{S}_x^k\left[\mathbb{S}_{x+\mu}^k, \mathbb{S}_z^3\right]\right] \tag{6.14}$$

$$= J\sum_{x,\mu}\left[i\epsilon^{j3l}\mathbb{S}_x^l\mathbb{S}_{x+\mu}^j + \mathbb{S}_x^k i\epsilon^{k3m}\mathbb{S}_{x+\mu}^m\right] \tag{6.15}$$

$$= J\sum_{x,\mu}\left[\mathbb{S}_x^l\mathbb{S}_{x+\mu}^j\right]\left(i\epsilon^{j3l} + i\epsilon^{l3j}\right) \tag{6.16}$$

$$= 0. \tag{6.17}$$

In terms of the world lines, the magnetization is proportional to the difference between the number of spin up world lines and spin down world lines. Just as in the analogous

situation in chapter 4, the weights appearing for winding clusters arise because it is these clusters which change the magnetization.

Using this choice of quantization axis leads to the same sort of problem as occurred in section 4.3. As the lattice becomes larger in the time direction, it becomes increasingly rare that such winding clusters exists. The algorithm is not efficient at updating this winding number, despite its physical significance.

Quantizing Transverse to the Field

When the quantization axis is chosen to be transverse to the field, $\mathbb{M}$ can be given by[1]

$$\mathbb{M} = e^{\epsilon B \mathbb{S}_1} = e^{\frac{\epsilon B}{2}\sigma_1} = \begin{bmatrix} \cosh\left(\frac{\epsilon B}{2}\right) & \sinh\left(\frac{\epsilon B}{2}\right) \\ \sinh\left(\frac{\epsilon B}{2}\right) & \cosh\left(\frac{\epsilon B}{2}\right) \end{bmatrix} \tag{6.18}$$

$$= e^{-\frac{\epsilon B}{2}} \begin{bmatrix} 1 & 0 \\ 0 & 1 \end{bmatrix} + \sinh\left(\frac{\epsilon B}{2}\right) \begin{bmatrix} 1 & 1 \\ 1 & 1 \end{bmatrix}, \tag{6.19}$$

or expanding to first order in ϵ,

$$\mathbb{M} \approx \begin{bmatrix} 1 & \frac{\epsilon B}{2} \\ \frac{\epsilon B}{2} & 1 \end{bmatrix} = \left(1 - \frac{\epsilon B}{2}\right) \begin{bmatrix} 1 & 0 \\ 0 & 1 \end{bmatrix} + \frac{\epsilon B}{2} \begin{bmatrix} 1 & 1 \\ 1 & 1 \end{bmatrix}. \tag{6.20}$$

The appearance of non-zero off-diagonal elements in this matrix signals the breaking of the clusters. Now there are two breakups for the $\mathbb{M}$ links; the sites may be bonded or not, as shown in table 6.1. The simple structure of this decomposition is summarized in table 6.2.

Because the clusters can now break open, the argument for the cancellations used when the clusters were closed loops fails again. A typical configuration for a 1+1 dimensional version of this system is shown in fig. 6-2. The horizontal breakup still has its signs, and so the horizontal bonds still change the global sign when they are flipped. Thus, with open clusters in which there can be any number of horizontal

[1] As with h in chapter 4, B shall be taken to be positive w.l.o.g.

Matrix	Diagram	Allowed configurations
$\begin{bmatrix} 1 & 0 \\ 0 & 1 \end{bmatrix}$		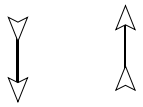
$\begin{bmatrix} 1 & 1 \\ 1 & 1 \end{bmatrix}$		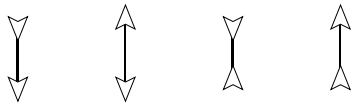

Table 6.1: *The bonded and unbonded breakups for the extra slice in the Heisenberg antiferromagnet in a magnetic field. None of these breakup segments have signs associated with them.*

Typical Spins	Total Weight	$1-\frac{\epsilon B}{2}$	$\frac{\epsilon B}{2}$
	1	+	+
	$\frac{\epsilon B}{2}$		+

Table 6.2: *The assignment of weights to the breakups for the extra slice in the antiferromagnetic Heisenberg model. The structure is the same as in table 4.2.*

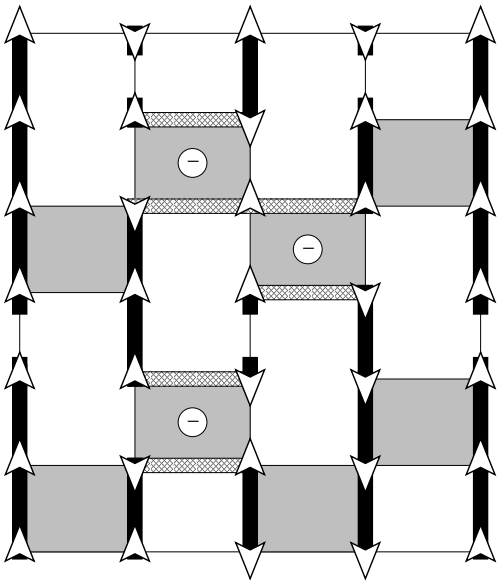

Figure 6-2: *A typical cluster configuration for the antiferromagnetic Heisenberg model with magnetic field $\vec{B}$ when the spins are quantized along an axis transverse to $\vec{B}$. This configuration has two merons, one of which is oriented against the reference configuration, hence its global sign should be negative. Flipping the cluster has flipped three horizontal segments carrying minus signs. This in turn has resulted in three plaquettes changing from the reference configuration to configurations which have signs. All other plaquettes contribute positive signs. The product of these signs is indeed negative, hence the meron calculation is correct.*

bonds, there may be merons. However, because the global sign can still be written in terms of merons, the meron cluster algorithm again suffices to solve the sign problem. This situation is very much analogous to that described in section 4.4.3.

6.3 Numerical Results

The meron algorithm for the spin ladders thus designed was implemented by S. Chandrasekharan and applied on several lattices, and numerical estimates were thus generated for the magnetization [18]. In order to demonstrate the inefficiency of the loop cluster algorithm which results from quantizing the spins on an axis parallel to the field, that algorithm and the meron algorithm were compared on a relatively small

lattice. The meron algorithm was then run on two larger lattices and used to generate estimates of the magnetization which can be compared with the known results from (1+1)D $O(3)$.

6.3.1 The Inefficiency of the Loop Algorithm

Both the loop algorithm and the meron algorithm were run on lattices with $L = L' = 8$, and $\beta J = 10$. The lattice was initially configured so as to have a large magnetization while the field was kept relatively weak. The moderate field was chosen so as to instigate an inefficiency, but not to support the very strong magnetization of the initial configuration. As each algorithm runs, the configuration of the lattice progresses toward thermal equilibrium and so the initial magnetization fades. The inefficiency of the loop algorithm is clear in that the number of sweeps required for the initial extreme magnetization to fade away is very large. In comparison, the magnetization equilibrates almost immediately using the meron algorithm. The magnetization is plotted as a function of the number of sweeps for the two algorithms and for two different values of the field in fig. 6-3. For the latter of the two cases, when $B = J$, the loop algorithm takes more than 100000 sweeps to reach equilibrium while the meron cluster algorithm has no thermalization problem.

By comparing the graphs one can see that the inefficiency of the loop algorithm becomes worse as the strength of the field grows. It is true that the loop algorithm can work tolerably when the magnetic field is very weak. However, as the field becomes stronger the loop algorithm becomes grossly impractical and in order to proceed it is necessary to use another method, such as the meron algorithm.

6.3.2 Comparison with (1+1)D $O(3)$

The meron algorithm was run to evaluate the response of the magnetization of the spin ladder to the magnetic field for two different lattice sizes. Values of ϵ were chosen small enough that the results generated are indistinguishable from the time continuum limit within statistical errors.

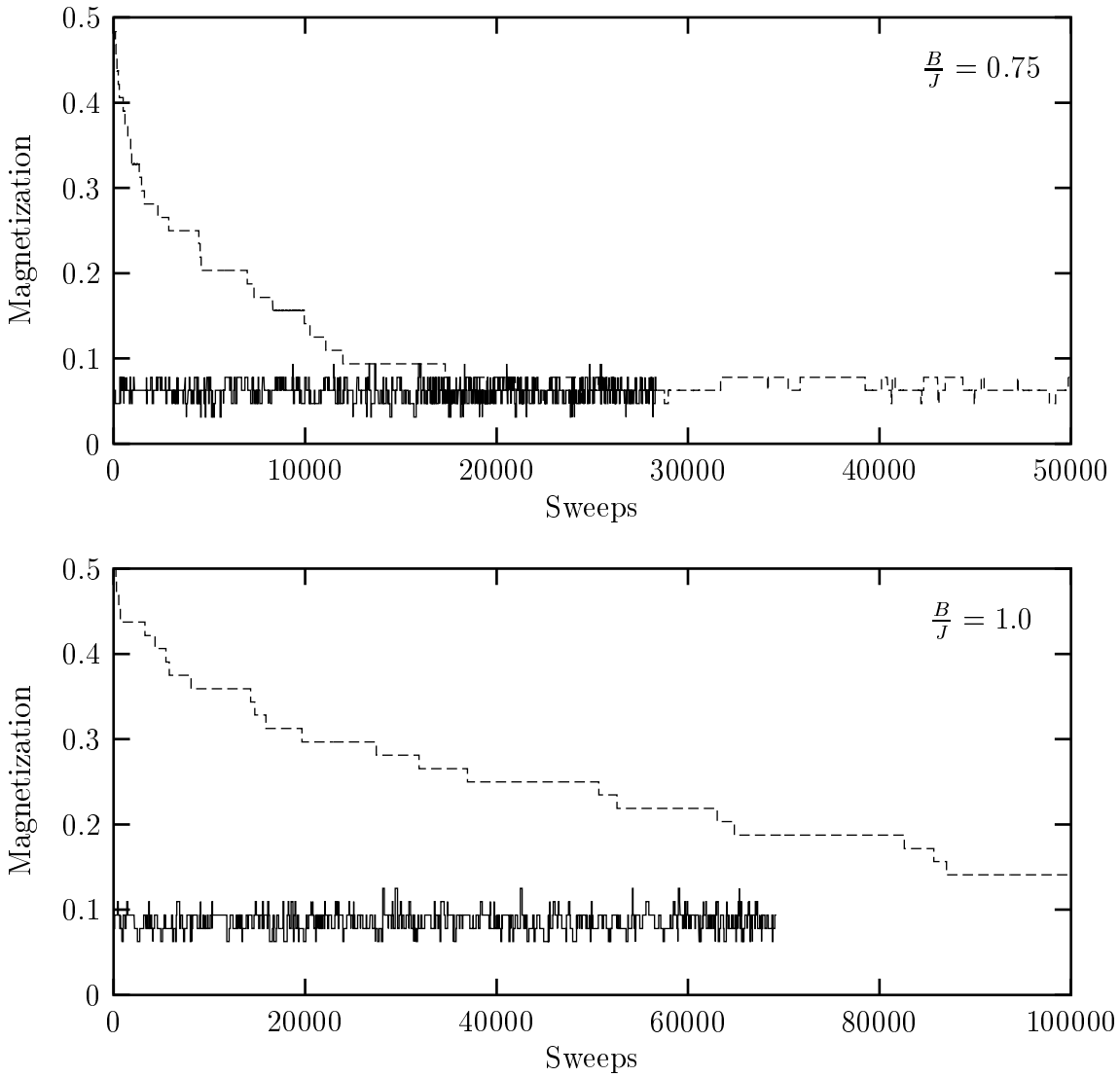

Figure 6-3: *A comparison of thermalization between the two choices of quantization axis for the Heisenberg quantum antiferromagnet in a magnetic field. The magnetization is shown with solid lines for the meron algorithm used when the quantization axis is transverse to the field, and with dashed lines for the loop cluster algorithm used when the quantization axis is parallel to the field. The first graph is for a magnetic field* $B = 0.75J$ *and the second graph is for* $B = J$.

L	βJ	ϵ	$\frac{B}{J}$	$\frac{\langle M^1 \rangle}{L}$
20	15	0.075	0.10	0.0048(4)
20	15	0.075	0.20	0.0184(4)
20	15	0.075	0.30	0.0452(8)
20	15	0.075	0.40	0.086(2)
20	15	0.075	0.50	0.120(4)
20	15	0.075	1.00	0.324(4)
20	15	0.075	2.00	0.76(2)
20	15	0.075	3.00	1.280(8)
20	15	0.075	4.00	1.93(3)
20	15	0.075	4.20	2.000(8)
20	15	0.075	4.40	2.000(8)
40	24	0.08	0.10	0.00104(8)
40	24	0.08	0.20	0.0096(6)
40	24	0.08	0.30	0.042(2)
40	24	0.08	0.40	0.085(3)
40	24	0.08	0.50	0.117(7)
40	24	0.08	1.00	0.332(4)

Table 6.3: *Numerical results for the magnetization density* $\frac{\langle M^1 \rangle}{L}$ *for two lattice sizes* ($L = 20$, $\beta J = 15$) *and* ($L = 40$, $\beta J = 24$). *In both cases* $L' = 4$.

Using the inverse correlation length $m = 0.141(2)$ from [48] and the magnon velocity $c = 1.657(2)$ from [5], the results calculated with the meron algorithm can be compared to the known exact results both for the infinite volume zero temperature limit and for finite size and temperature. The data generated is summarized in table 6.3, and shown in fig. 6-4. Considering that the data were generated on lattices with $L' = 4$ while the analytic expressions were derived in the large L' limit, the agreement of the numerical data with the theoretical results is quite remarkable.

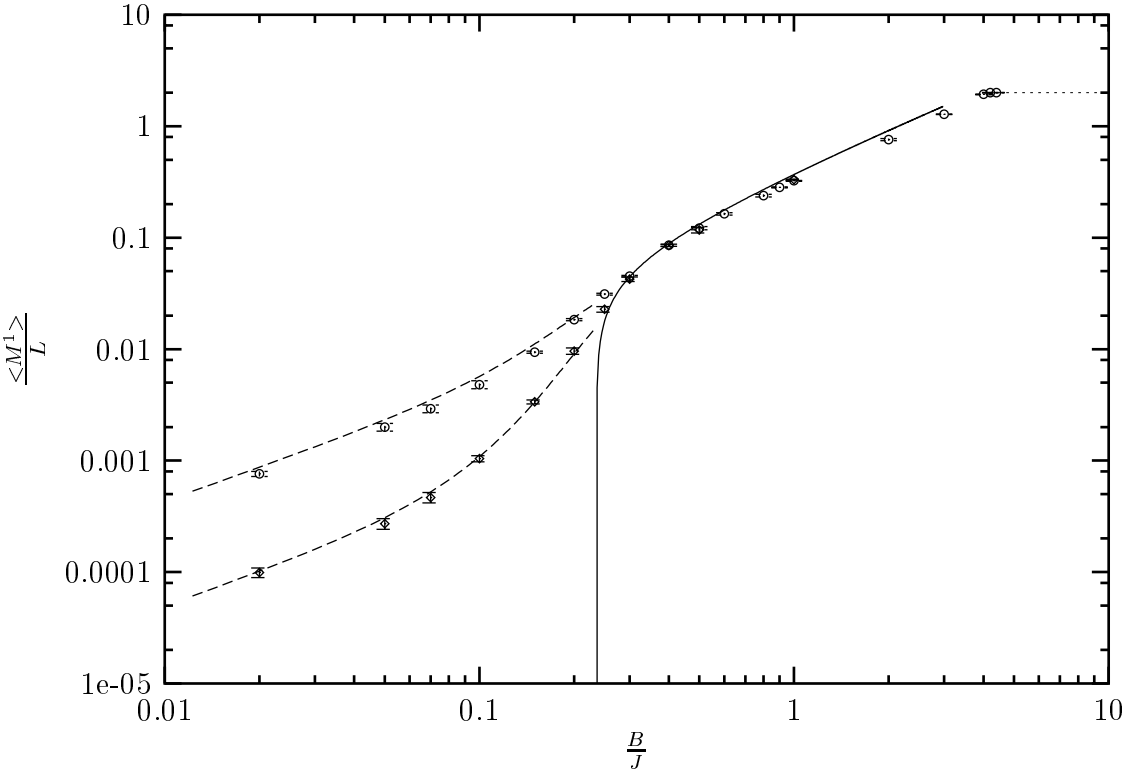

Figure 6-4: *Magnetization density* $\langle M^1 \rangle / L$ *of quantum spin ladders consisting of* $L' = 4$ *coupled chains as a function of the magnetic field* B*. The numerical data are for two systems: one of size* $L = 20$ *at inverse temperature* $\beta J = 15$ *(circles) and the other for* $L = 40$ *at* $\beta J = 24$ *(diamonds). The solid curve is the infinite volume, zero temperature analytic result, while the two dashed curves are finite volume, non-zero temperature analytic results for the two simulated systems in the small* B *region. The dotted curve represents saturation of the magnetization per spin at* $1/2$*.*

Chapter 7

Conclusions

7.1 Summary and Interpretation

Monte Carlo integration is the most effective tool currently available for studying strongly coupled systems, but the introduction of a chemical potential to these systems renders the traditional formulation of this tool ineffective because of complex action problems. The class of physical systems for which numerical study is thus unavailable includes both systems which are ubiquitous – such as finite density nuclear matter – and systems which are potentially of great utility – such as high T_c superconductors. The lack of effective tools for studying strongly coupled systems in the presence of chemical potentials is thus a significant hindrance because it obstructs the understanding of important physical systems.

In an effort to understand this hindrance and learn how to circumvent it, two similar models which exhibit sign problems – but are otherwise well understood – were chosen for study: the D-Theory representation of 1+1 dimensional $O(3)$ field theory with chemical potential and the Heisenberg quantum antiferromagnet in a magnetic field. These models provided an arena in which the sign problem could be attacked without the distractions inherent in more complex systems. With the sign problem thus separated from other difficulties in a limited environment in which the arsenal of cluster techniques could be brought to bear, it was possible to eliminate the problem completely.

Both of the models considered can manifest their inefficiency in different ways depending on the choice of the quantization axis.

An axis parallel to the chemical potential appears at first to be the most natural choice; the particle number is then measured with a diagonal operator and the relation between the spins on the lattice and the charge coupled to the chemical potential is readily apparent in terms of spin world lines. This choice, however, does not sufficiently involve the chemical potential with the cluster algorithm. Unless a cluster happens to be constructed which winds around the lattice, the chemical potential does not enter a simulation at all. Thus the algorithms which result from this choice of quantization axis are not efficient – they encounter severe autocorrelation problems.

If, instead, the spins are quantized along an axis transverse to the field, the world line interpretation fails and a sign problem is introduced. Without meron cluster techniques, this sign problem renders this choice of quantization axis as inefficient as the previous one. However, by decomposing the global sign in each configuration in terms of factors attributable to individual clusters, the sign problem can be brought under control. All cancellation can be forced to occur explicitly, and thus the corruption of the importance sampling ensemble introduced with the sign problem can be eliminated. With an accurate weight thus assigned to each configuration – one reflecting the configuration's final significance – importance sampling can proceed unimpeded. Thus is the sign problem solved.

The meron technique has proven to be very effective. The data generated measuring the particle number and magnetization using the meron algorithms match the corresponding theoretical predictions quite well, and statistical errors are well under control.

This investigation of the nature of sign problems has proven to be very fruitful. For the first time, a severe sign problem which appears because of a chemical potential has been completely solved. The considerable precision and accuracy of the numerical data generated by the meron algorithm attests to the effectiveness of the meron technique.

This success can be taken as evidence not only that sign problems can be solved

using meron clusters, but more broadly both of the power of cluster techniques in general and of the validity of D-Theory. The algorithmic flexibility to be gained by using cluster techniques to represent physical systems is not to be underestimated. Moreover, the D-Theory construction used to apply the cluster techniques to the (1+1)D $O(3)$ model – despite its apparent complexity – has been demonstrated to work as intended, finally producing numerical results in accordance with the original continuum theory.

7.2 Future Directions

Having solved a sign problem and thus simulated these simple systems at non-zero chemical potential, one would like next to apply the techniques developed here to more immediately relevant examples such as QCD and the Hubbard model. At present, the tools presented in this thesis and the associated cluster technology is not yet well enough developed to solve the complex action problems in those systems.

QCD as yet lacks an efficient cluster algorithm, and so the framework for applying meron methods is incomplete. There are D-Theory formulations for QCD in particular and for gauge theories in general [13, 19], but so far attempts to construct an efficient cluster algorithm for the simplest case – $U(1)$ gauge theory – have not met with success. That obstacle is the next challenge along the route to applying the methods presented here directly to simulate dense quark matter. Even with that obstacle remaining, the lessons learned in this study should provide a useful vantage point from which to understand the complex action problem in QCD. The fundamental notion of eliminating the false measure of importance in a Markov process by using improved estimators is more general than the meron cluster techniques which have been used in this thesis to implement that notion. Thus even if it should turn out that these techniques are not applicable in whole then they may well still be applicable in part.

The Hubbard model in the presence of a chemical potential, which may be usable to model high T_c superconductors, also suffers from a sign problem. For the case

of interest for superconductors – when the fermions in the model are repulsive – it is possible to construct a cluster algorithm and attribute sign changes to merons, but in the constructions currently known the resulting clusters do not conform to a reference configuration. Without a reference configuration, an absence of merons does not necessarily imply the global sign is positive. Thus merons can not be used to solve this sign problem until either the present understanding of the necessity of a reference configuration is extended, or a different cluster algorithm for the model is found.

The realm of possible algorithms based on the cluster concept is large and as yet only a small fraction of it has been explored. There is a good deal of flexibility in the construction of cluster algorithms, and there are many potential avenues to investigate. The notion of a reference configuration, for instance, is quite narrow as used here. In frustrated systems – such as the triangular lattice antiferromagnet – there is no reference configuration as they are currently understood. There may well be some more general idea which can be used in more cases. Similarly, the bonds used in the cluster models in this thesis were very restrictive – given two bonded spins and a state for one of the spins, the state of the other is completely determined. Loosening restriction may well allow the construction of cluster algorithms for a broader class of systems. The more the applicability of cluster methods can be broadened, the greater the range of models in which the meron concept can be used will grow.

Bibliography

[1] I. Affleck, T. Kennedy, E. Lieb, and H. Tasaki. Rigorous results on valence bond ground states in antiferromagnets. *Phys. Rev. Lett.*, 59:799–802, 1987.

[2] I. Affleck, T. Kennedy, E. Lieb, and H. Tasaki. Valence bond ground states in isotropic quantum antiferromagnets. *Commun. Math. Phys.*, 115:477, 1988.

[3] M. Alford. Color superconductivity in dense quark matter. *to appear in Proceedings of TMU-Yale*, Dec. 1999, hep-ph/0003185.

[4] M. Alford, K. Rajagopal, and F. Wilczek. QCD at finite baryon density: Nucleon droplets and color superconductivity. *Phys. Lett.*, B422:247, 1998, hep-ph/9711395.

[5] B. B. Beard, R. J. Birgeneau, M. Greven, and U. J. Wiese. The square lattice Heisenberg antiferromagnet at very large correlation lengths. *Phys. Rev. Lett.*, 80:1742–1745, 1997, cond-mat/9709110.

[6] B. B. Beard, R. Brower, S. Chandrasekharan, D. Chen, A. Tsapalis, and U. J. Wiese. D-Theory: Field theory via dimensional reduction of discrete variables. *Nucl. Phys. Proc. Suppl.*, 63:775, 1998, hep-lat/9709120.

[7] B. B. Beard and U. J. Wiese. Simulations of discrete quantum systems in continuous Euclidean time. *Phys. Rev. Lett.*, 77:5130–5133, 1996.

[8] B. B. Beard and U. J. Wiese. Simulations of discrete quantum systems in continuous Euclidean time. *Nucl. Phys. Proc. Suppl.*, 53:838–840, 1997, cond-mat/9602164.

[9] H. Bethe. On the theory of metals. 1. Eigenvalues and eigenfunctions for the linear atomic chain. *Z. Phys.*, 71:205–226, 1931.

[10] W. Bietenholz, A. Pochinsky, and U. J. Wiese. Meron cluster simulation of the theta vacuum in the 2-d $O(3)$ model. *Phys. Rev. Lett.*, 75:4524–4527, 1995, hep-lat/9505019.

[11] W. Bietenholz, A. Pochinsky, and U. J. Wiese. Testing Haldane's conjecture in the $O(3)$ model by a meron cluster simulation. *Nucl. Phys. Proc. Suppl.*, 47:727–730, 1996, hep-lat/9509053.

[12] R. Brower, S. Chandrasekharan, and U. J. Wiese. Green's functions from quantum cluster algorithms. *Physica*, A261:520, 1998, cond-mat/9801003.

[13] R. Brower, S. Chandrasekharan, and U. J. Wiese. QCD as a quantum link model. *Phys. Rev.*, D60(094502), 1999, hep-th/9704106.

[14] S. Chakravarty, B. I. Halperin, and D. R. Nelson. Low-temperature behavior of two-dimensional quantum antiferromagnets. *Phys. Rev. Lett.*, 60:1057, 1988.

[15] S. Chakravarty, B. I. Halperin, and D. R. Nelson. Two-dimensional quantum Heisenberg antiferromagnet at low temperatures. *Phys. Rev.*, B39:2344, 1988.

[16] S. Chandrasekharan. Fermion cluster algorithms. *Nucl. Phys. Proc. Suppl.*, 83:774–776, 2000, hep-lat/9909007.

[17] S. Chandrasekharan, J. Cox, K. Holland, and U. J. Wiese. Meron-cluster simulation of a chiral phase transition with staggered fermions. *Nucl. Phys.*, B576:481, 2000, hep-lat/9906021.

[18] S. Chandrasekharan, B. Scarlet, and U. J. Wiese. Meron-cluster simulation of quantum spin ladders in a magnetic field. 1999, cond-mat/9909451.

[19] S. Chandrasekharan and U. J. Wiese. Quantum link models: A discrete approach to gauge theories. *Nucl. Phys.*, B492:455–474, 1997, hep-lat/9609042.

[20] S. Chandrasekharan and U. J. Wiese. Meron-cluster solution of a fermion sign problem. *Phys. Rev. Lett.*, 83:3116–3119, 1999, cond-mat/9902128.

[21] S. Coleman. There are no Goldstone bosons in two-dimensions. *Commun. Math. Phys.*, 31:259–264, 1973.

[22] J. Cox, C. Gattringer, K. Holland, B. Scarlet, and U. J. Wiese. Meron-cluster solution of fermion and other sign problems. *Nucl. Phys. Proc. Suppl.*, 83:777–791, 2000, hep-lat/9909119.

[23] M. Creutz. Confinement and the critical dimensionality of space-time. *Phys. Rev. Lett.*, 43:553–556, 1979.

[24] M. Creutz. *Quarks, gluons, and lattices.* Cambridge University Press, 1983.

[25] M. Creutz. *Quantum fields on the computer.* World Scientific, 1992.

[26] E. Dagotto and T. M. Rice. Surprises on the way from one- to two-dimensional quantum magnets: The ladder materials. *Science*, 271:618–623, 1996.

[27] H. G. Evertz, G. Lana, and M. Marcu. Cluster algorithm for vertex models. *Phys. Rev. Lett.*, 70:875–879, 1993, cond-mat/9211006.

[28] C. Fortuin and P. Kasteleyn. On the random-cluster model I. *Physica*, 57:536–564, 1972.

[29] F. D. M. Haldane. Continuum dynamics of the 1-d Heisenberg antiferromagnetic identification with the $O(3)$ nonlinear sigma model. *Phys. Lett.*, A93:464–468, 1983.

[30] F. D. M. Haldane. Nonlinear field theory of large spin Heisenberg antiferromagnets. Semiclassically quantized solitons of the one-dimensional easy axis Néel state. *Phys. Rev. Lett.*, 50:1153–1156, 1983.

[31] P. Hasenfratz and H. Leutwyler. Goldstone boson related finite size effects in field theory and critical phenomena with $O(N)$ symmetry. *Nucl. Phys.*, B343:241–284, 1990.

[32] P. Hasenfratz, M. Maggiore, and F. Niedermayer. The exact mass gap of the $O(3)$ and $O(4)$ non-linear sigma models in $d = 2$. *Phys. Lett.*, B245:522–528, 1990.

[33] P. Hasenfratz and F. Niedermayer. The exact mass gap of the $O(N)$ sigma model for arbitrary N is $>= 3$ in $d = 2$. *Phys. Lett.*, B245:529–532, 1990.

[34] P. Hasenfratz and F. Niedermayer. The exact correlation length of the antiferromagnetic $d = (2 + 1)$ Heisenberg model at low temperatures. *Phys. Lett.*, B268:231–235, 1991.

[35] V. A. Kashurnikov, N. V. Prokof'ev, B. V. Svistunov, and M. Troyer. Quantum spin chains in a magnetic field. *Phys. Rev.*, B59:1162–1167, 1999.

[36] D. V. Khveshchenko. Singlet pairing in the double-chain t-J model. *Phys. Rev.*, B50:380, 1994, cond-mat/9401011.

[37] E. Lieb, T. Schultz, and D. Mattis. Two soluble models of an antiferromagnetic chain. *Ann. Phys.*, 16:407–466, 1961.

[38] N. D. Mermin and H. Wagner. Absence of ferromagnetism or antiferromagnetism in one-dimensional or two-dimensional isotropic Heisenberg models. *Phys. Rev. Lett.*, 17:1133–1136, 1966.

[39] W. H. Press, S. A. Teukolsky, W. T. Vertterling, and B. P. Flannery. *Numerical Recipes in C, The Art of Scientific Computing*, chapter 18. Cambridge University Press, second edition, 1997.

[40] N. V. Prokof'ev, B. V. Svistunov, and I. S. Tupitsyn. Exact quantum Monte Carlo process for the statistics of discrete systems. *JETP Lett.*, 64:911–916.

[41] N. V. Prokof'ev, B. V. Svistunov, and I. S. Tupitsyn. Exact, complete, and universal continuous-time worldline Monte Carlo approach to the statistics of discrete quantum systems. *Sov. Phys. JETP*, 87:310, 1998, cond-mat/9703200.

[42] N. V. Prokof'ev, B. V. Svistunov, and I. S. Tupitsyn. "worm" algorithm in quantum Monte Carlo simulations. *Phys. Lett.*, A238:253–257, 1998.

[43] K. Rajagopal. Mapping the QCD phase diagram. *Nucl. Phys.*, A661:150, 1999, hep-ph/9908360.

[44] R. Rapp, T. Schafer, E. V. Shuryak, and M. Velkovsky. Diquark Bose condensates in high density matter and instantons. *Phys. Rev. Lett.*, 81:53–56, 1998, hep-ph/9711396.

[45] A. Sandvik. Stochastic series expansion method with operator-loop update. *Phys. Rev.*, B59:R14157–R14160.

[46] G. Sierra. The non-linear sigma model and spin ladders. *J. Phys.*, A29:3299–3310, 1996, cond-mat/9512007.

[47] R. H. Swendsen and J. S. Wang. Nonuniversal critical dynamics in Monte Carlo simulations. *Phys. Rev. Lett.*, 58:86–88, 1987.

[48] O. F. Syljuasen, S. Chakravarty, and M. Greven. Correlation lengths in quantum spin ladders. *Phys. Rev. Lett.*, 78:4115–4118, 1997, cond-mat/9701197.

[49] S. R. White, R. M. Noack, and D. J. Scalapino. Resonating valence bond theory of coupled Heisenberg chains. *Phys. Rev. Lett.*, 73:886, 1994.

[50] P. B. Wiegmann. Exact solution of the $O(3)$ nonlinear sigma model. *Phys. Lett.*, B152:209, 1985.

[51] U. J. Wiese. Quantum spins and quantum links: The D-Theory approach to field theory. *Nucl. Phys. Proc. Suppl.*, 73:146, 1999, hep-lat/9811025.

[52] U. J. Wiese and H. P. Ying. A determination of the low energy parameters of the 2-d Heisenberg antiferromagnet. *Z. Phys.*, 93:147–150, 1994.

[53] U. Wolff. Collective Monte Carlo updating for spin systems. *Phys. Rev. Lett.*, 62:361, 1989.

[54] U. Wolff. Asymptotic freedom and mass generation in the $O(3)$ nonlinear sigma model. *Nucl. Phys.*, B334:581–610, 1990.

Index